Mon. Not. R. Astron. Soc. **000**, 1–19 (2002) Printed 22 March 2011 (MN LATEX style file v2.2)

Star formation history of barred disc galaxies

P. Sánchez-Blázquez[1,2,3,4] ⋆ P. Ocvirk[5,6], B. K. Gibson[4], I. Pérez[7], R.F. Peletier[8]
[1] *Departamento de Física Teórica, Universidad Autónoma de Madrid, E-28049, Cantoblanco, Madrid, Spain*
[2] *Instituto de Astrofísica de Canarias, E-38200 La Laguna, Tenerife, Spain*
[3] *Departamento de Astrofísica, Universidad de La Laguna, E-38205 La Laguna, Tenerife, Spain*
[4] *Jeremiah Horrocks Institute, University of Central Lancashire, Preston, PR1 2HE, UK*
[5] *Astrophysikalisches Institut Potsdam, an der Sternwarte 16, D-14482 Postdam, Germany*
[6] *Observatoire Astronomique de Strasbourg, 11 rue de l"université, 67000 Strasbourg, France*
[7] *Departamento de Física Teórica y del Cosmos Universidad de Granada, E-18071, Granada, Spain*
[8] *Kapteyn Astronomical Institute, Rijksuniversiteit Groningen, 9700 AV Groningen, The Netherlands*

ABSTRACT

We present the first results of a pilot study aimed at understanding the influence of bars on the evolution of galaxy discs through the study of their stellar content. We examine here the kinematics, star formation history, mass-weighted, luminosity-weighted, and single stellar population (SSP) equivalent ages and metallicities for four galaxies ranging from lenticulars to late-type spirals. The data employed extends to 2-3 disc scalelengths, with S/N(Å)>50. Several techniques are explored to derive star formation histories and SSP-equivalent parameters, each of which are shown to be compatible. We demostrate that the age-metallicity degeneracy is highly reduced by using spectral fitting techniques –instead of indices– to derive these parameters. Our results are robust to the choices of stellar population models. We found that the majority of the stellar mass in our sample is composed of old (∼10 Gyr) stars. This is true in the bulge and the disc region, even beyond two disc scalelengths. In the bulge region, we find that the young, dynamically cold, structures produced by the presence of the bar (e.g., nuclear discs or rings) are responsible for shaping the bulges' age and metallicity gradients, as suggested by Peletier et al. (2007). In the disc region, a larger fraction of young stars is present in the external parts of the disc compared with the inner disc. The disc growth is, therefore, compatible with a moderate inside-out formation scenario, where the luminosity-weighted age changes from ∼10 Gyrs in the centre, to ∼4 Gyrs at two disc scalelengths, depending upon the galaxy. However, the presence of substructure, like star forming rings, can produce stellar population trends that are not directly related with the growing of the disc but to the bar potential. For two galaxies, we compare the metallicity and age gradients of the disc major axis with that of the bar, finding very important differences. In particular, the stellar population of the bar is more similar to the bulge than to the disc, indicating that, at least in those two galaxies, bars formed long ago and have survived to the present day.

Key words: galaxies: stellar content – galaxies: spiral – galaxies: evolution – galaxies: abundances – galaxies: kinematics and dynamics

1 INTRODUCTION

During disc assembly, secular evolution must have played a role in shaping the structure of disc galaxies as we see them at z=0. Non-axisymmetric instabilities, particularly bars, drive a substantial redistribution of mass and angular momentum in the disc (Sellwood & Wilkinson 1993; Sellwood 1981; Pfenniger & Friedli 1991; Athanassoula 2003; Debattista et al. 2006). Since bars appear to affect strongly the overall dynamics and evolution of galaxies, it is reasonable to presume that they also play a significant role in shaping galactic chemical evolution, since mixing by global gas flows will clearly change abundance profiles in the disc (see Friedli 1998; Roskar et al. 2008b; Sánchez-Blázquez et al. 2009a); for example, numerical simulations (Friedli, Benz & Kennicutt 1994) predict that the stellar abundance gradient in disc galaxies is flattened by macroscopic mixing induced by the bar. The slope of the abundance gradients in both the stellar and gaseous component are reduced in a few dynamical timescales by more than 50%.

⋆ E-mail: psanchezb@iac.es

Several of the relationships observed in our own Galaxy used to constrain chemical evolution models, such as the age-metallicity relation (Edvardsson et al. 1993; Carraro et al. 1998; Feltzing & Gonzalez 2001; Rocha-Pinto et al. 2000; Twarog 1980ab; Feltzing et al. 2001), the metallicity distribution of G- and K-dwarf stars (e.g., Rocha-Pinto & Maciel 1996; Wyse & Gilmore 1995; Flynn & Morell 1997; Favata et al. 1997; Haywood 2001) or the temporal evolution of metallicity gradients (Friel et al. 2002; Maciel et al. 2003; Stanghellini et al. 2006; Magrini et al. 2009) could be strongly influenced by the presence of radial migrations.

The mechanisms proposed for being primary drivers of radial migration are numerous (Spitzer & Schwarzschild 1953; Barbanis & Woltjer 1967; Friedli 1998; Binney & Lacey 1988; Fuchs 2001; Sellwood & Binney 2002; Roskar et al. 2008a; Sánchez-Blázquez et al. 2009; Minchev & Falmaey 2009). However, in the present work we are interested in constraining the influence of a bar upon this migration. This is important, not only because the Milky Way has a bar, but because recent simulations suggest that the interaction between the bar and the spiral structure can result in significantly faster angular momentum changes, making mixing mechanisms due to spiral arms much more efficient in barred than in non-barred galaxies (Minchev & Falmaey 2009).

Several studies have found that barred galaxies have a shallower gas-phase metallicity gradient than non-barred ones (e.g., Pagel & Edmunds 1981; Vila-Costas & Edmunds 1992; Edmunds & Roy 1993; Martin & Roy 1994; Zaritsky et al. 1994; Ryder 1995). However, an equivalent study for the stellar abundances remains to be done. Studies of the gas-phase abundances provide with a present-day snapshot of the interstellar medium abundances. On the other hand, study of the stellar ages and metallicities give us 'archaeological' clues as to the chemical and dynamical evolution of the galactic structures. It is very important to study both because gas and stars suffer from very different evolutionary processes; the gas is mainly dominated by the gravitational torque of the non-axisymmetric mass component, while the evolution of the stellar component is mainly affected by different orbital mixing.

In general, stellar population studies in the disc region of spiral galaxies are sparse, with exception of our own galaxy (see Freeman & Bland-Hawthorn 2002 for a review; Friel et al. 2002; Yong et al. 2006; Carraro et al. 2007) and for some nearby galaxies, such as M33 (Monteverde et al. 1997; Barker et al. 2008; Williams et al. 2009; Cioni et al. 2009), M100 (Beauchamp & Hardy 1997); M81 (Hughes et al. 1994; Tikhonov et al. 2005; Williams et al. 2008; Davdige 2006a, 2008); NGC2403 (Davidge 2007); NGC 300 (Vlajic et al. 2008; Kudritzki et al 2008; Urbaneja et al. 2005; Gogarten et al. 2010) or M31 (Worthey et al. 2005). For external galaxies outside the Local Group, stellar population gradients have been mainly investigated using (mostly optical) colours (e.g., de Jong 1996; Peletier & Balcells 1996; Jansen et al 2000; Bell & de Jong 2000; MacArthur et al. 2004; Taylor et al. 2005; Muñoz-Mateos et al. 2007, 2009 (using UV-GALEX colours); Prochaska et al. 2010). These studies found that disc galaxies tend to be bluer in the external parts. This trend has been interpreted as the consequence of stellar population gradients, in the sense that galaxies are older and more metal rich in their centers than in the external parts. However, there are large discrepancies in the magnitude of the stellar population gradients derived by different authors. This is because it is extremely difficult to disentangle the effects of age, metallicity, and dust extinction (on average, $\sim$1 mag in the central regions, see Ganda et al. 2009) using only colours. Spectroscopic studies may help to alleviate the associated degeneracies, but the low-surface brightness of the disc region and the nebular emission lines filling some of the most important age-diagnostic absorption lines make these studies very difficult. Some pioneering works tried to overcome the difficulty of measuring low-surface brightness absorption lines in the disc using narrow-band imaging, or performing Fabry-Pérot interferometry with Tunable Filters (Beauchamp & Hardy 1997; Molla, Hardy & Beauchamp 1999; Ryder, Fenner & Gibson 2005). Unfortunately, the low spectral resolution and poor S/N ratio of the data compromised the results in each case. Furthermore, these works were restricted to the study of just a few indices (Mgb, Fe5270, Fe5335) which limited their ability to break the age-metallicity degeneracy. More recently, Yoachim & Dalcanton (2008), and MacArthur, González & Courteau (2009) have measured line-strength indices and star formation histories, repectively, as a function of radius using long-slit spectroscopy. While the former found very strong radial age gradients and flat metallicity gradients for the only galaxy for which they could derive stellar population gradients, (FGC 1440, and Scd galaxy), the latter reported very mild gradients in both age and metallicity.

These differences maybe the consequence of the very reduced samples (9 and 1 galaxy), although they can also be due to the different techniques used to derive stellar parameters in both studies –while the former obtained single stellar population (SSP hereafter)-equivalent parameters, the latter derived luminosity and mass-weighted values. The difference could also be due to the uncertainties of the emission-line corrections that affect more strongly the ages derived with single indices than those obtained with full spectral fitting. It is one of the motivation of this work to explore some of these issues. Despite heroic efforts, we really only have information pertaining to the inner disc for most galaxies ($\sim$1$-$2 scalelengths, in the MacArthur et al. 2009 data), and only for 9 galaxies.

This is part of a long-term project aimed at studying the star formation history of the different components of a sample of face-on disc galaxies with deep long-slit observations taken at the GEMINI telescope. One of our main goals is to understand the influence of bars on the evolution of these systems, for which, in a forthcoming paper we will compare with analogous non-barred galaxies. This study is complemented by that of the stellar populations in galaxy bars and their bulges (Pérez, Sánchez-Blázquez & Zurita 2007; Pérez, Sánchez-Blázquez & Zurita 2009; Pérez & Sánchez-Blázquez 2010, in preparation). In this paper, we present a pilot study using data from 4 galaxies. The aim of our work here is to present the different analysis techniques, their limitations and robustness, and the dependence of the results on the choice of different parameters.

2 OBSERVATIONS AND DATA REDUCTION

The galaxies were selected from the Third Reference Catalogue (RC3: de Vaucouleurs et al. 1991) to cover a range

in morphological types from S0 to Sc. They were imposed to be nearby ($cz < 3000$ kms^{-1}) and barred. For the earlier types, we selected the sample to overlap with that of Pérez, Sánchez-Blázquez & Zurita (2007) as, for these galaxies, spectra along the bar have already been obtained at Siding Spring Observatory and the Isaac Newton Telescope (Pérez et al. 2007, 2009). This will allow us to compare the gradients along the bar with those along the disc (see § 5.4).

All observations were taken with the Gemini South Multi-Object Spectrograph (GMOS) (Hook et al. 2004) as part of Gemini Programs GS-2008B-73 and GS-2008B-85. Long-slit spectroscopy along the major axes of the galaxies was obtained with a slit width of 0.75" with the B600-G5303 grating. We performed a 4×2 binning giving a spectral resolution of FWHM=3.5 Å (measured on the sky lines of the images) and a spatial scale of 0.146 arcsec/pixel. Our spectra cover the wavelength range 4050-6750 Å, with gaps between ∼4920-5025 and 5865-5930Å.

The major obstacle to measuring reliable stellar populations at large radii is the sky subtraction, as the light of the galaxy is only a few percent of the background. Nod-and-Shuffle spectroscopy allows very accurate sky subtraction and is available on GMOS. However, the length of the slit in this mode is only 1.83 arcmin and our objects span between 2 and 5 arcmin on the sky. In order to obtain a good sky subtraction after every target exposure of 1800s, a sky exposure of 400s was taken slightly offset (∼200 arcsec) from the target. Total exposure times for each galaxy were 1800×6 (3h), while a 400s exposure on the sky was taken before and after each target exposure. These long exposures on sky minimise the amount of noise introduced in this step.

Standard data reduction procedures (flat-fielding, cosmic ray removal, wavelength calibration, sky subtraction and fluxing) were performed with REDUCEME (Cardiel 1999)[1]. This reduction package allows a parallel treatment of data and error frames from the initial steps of the reduction process and, therefore, generates an associated error spectrum of each individual data spectrum which is quite realistic and takes into account the propagation of the errors in each reduction step. Initial reduction of the CCD frames involved bias and dark current subtraction, removal of pixel-to-pixel sensitivity variations (using flat-field exposures of a tungsten calibration lamp) and correction for two-dimensional low frequency scale sensitivity variations (using twilight sky exposures). Prior to the wavelength calibration, arc frames were used to correct for C-distortion in the images. Spectra were converted to a linear wavelength scale using typically 80 arc lines fitted by 3rd order polynomials, with RMS errors of ∼0.05Å. The images were not distorted in the spatial direction and, therefore, S-correction was not applied. Before performing any distortion correction or wavelength calibration, the sky images were multiplied by a factor corresponding to the exposure time of the science frames and were subtracted.

From each fully reduced galaxy frame, a final frame was created by extracting spectra along the slit, binning in the spatial direction to guarantee a minimum signal-to-noise ratio per Å (S/N) of 50 in a 50Å-wide region centered on 5100 Å. The spectroscopic data extend to ∼2 scalelengths for most of the galaxies, except for NGC 1358, where ∼3 scalelengths are reached. Only for two of the four galaxies (NGC 1358 and NGC 1365) do our data extend beyond corotation.

2.1 Notes on the Sample

- NGC 1358: This galaxy is a Seyfert, S0/a galaxy with a bar. For this galaxy, long-slit spectroscopy along the bar was presented in Pérez, Sánchez-Blázquez & Zurita (2009). The galaxy has an inner gaseous spiral structure (with size <1 kpc; Dumas, Emsellem & Ferruit 2007). The outer bar has a corotation radius of 5.1 kpc.
- NGC 1365: This galaxy is a barred SB(s)b galaxy. It has a nuclear ring with radius ∼ 7 arcsec. Several studies have reported super-solar metallicities in the gaseous components, measured in its HII regions (Roy & Walsh 1997).
- NGC 1433: A prototypical ringed barred galaxy (Treuthardt et al. 2008), with a morphological type (R')SB(r)ab. It has a circumnuclear ring with a diameter about 0.1 times the size of the bar (at r∼ 19", Crocker et al. 1996; Hameed & Devereuz 1999; Buta et al. 2001; Comeron et al. 2007), and an outer pseudo-ring about twice the diameter of the bar. Spectra along the bar were presented by Pérez et al. (2009).
- NGC 1672: An SB(s)b, barred spiral galaxy, with a circumnuclear ring of star formation at r∼0.350 kpc (Sérsic & Pastoriza 1965; Comeron et al. 2007) surrounding a nucleus with low-level activity (Veron-Cetty & Veron 1986), also containing a star forming region. The bar size is 5.1 kpc (Buta 1987) and the inner Lindblad resonance (ILR) is calculated to be 0.49 kpc from the galaxy center, coincident with the edge of the circumnuclear ring.

3 KINEMATICS, DYNAMICS AND EMISSION LINE REMOVAL

One of the most important drawbacks to studying the stellar population of disc galaxies has been that the stellar absorption line spectra are highly contaminated by nebular emission lines. However, this situation has changed with the development of new specialist software that allows the simultaneous fitting of absorption and emission lines. We used `GANDALF` (Sarzi et al. 2006) to perform this task. `GANDALF` fits simultaneously the absorption and emission lines treating the latter as additional Gaussians. In a first step, emission lines are masked and the absorption line spectrum is fit with the penalised pixel-fitting `pPXF` (Cappellari & Emsellem 2004), using as templates the new stellar population models of Vazdekis et al. (2010) based on the MILES library (Sánchez-Blázquez et al. 2006; Cenarro et al. 2007)[2]. In this step, radial velocities and velocity dispersions (σ, hereafter) for the stellar component are derived. The best values of velocity and σ and the best template mix are then used as initial values for the derivation of emission lines using `GANDALF`. Emission-line equivalent widths, radial velocities, and σ for the gaseous component are derived in this second step. The

[1] `www.ucm.es/info/Astrof/software/reduceme/reduceme.html`

[2] The models are available at `miles.iac.es`

gal	PA	i	Morph	r_e(kpc)	r_s (kpc)
(1)	(2)	(3)	(4)	(5)	(6)
NGC 1358	180	38.8 (iii)	SAB(R)0	1.17(a)	5.5(a)
NGC 1365	225	40.0(i)	(R')SBb(s)b	0.96(c)	6.5(b)
NGC 1433	210	33.0(ii)	(R)SB(rs)ab	0.26(c)	1.8(c)
NGC 1672	140	36.0 (iv)	(R')SB(r)bc	0.40(c)	1.6 (c)

Table 1. Sample of galaxies observed; columns: (1) galaxy name; (2) PA: Position angle of the slit in degrees from N through E; (3) inclination in degrees (obtained from different references) (i) Roy & Walsh (1997) (ii) Ryder et al. (1996) (iii) Dumas, Emsellem & Ferruit (2007) (iv) Baumgart & Peterson (1986); (4) Morphological type (from Hyperleda); (5) effective radius of the bulge; (6) scalelength of the disc. The references for the effective radius and the scale-length of the disc are the following: (a) Dong & de Robertis (2006); (b) Zánmar-Sánchez et al. (2008); (c) Baumgart & Peterson (1986).

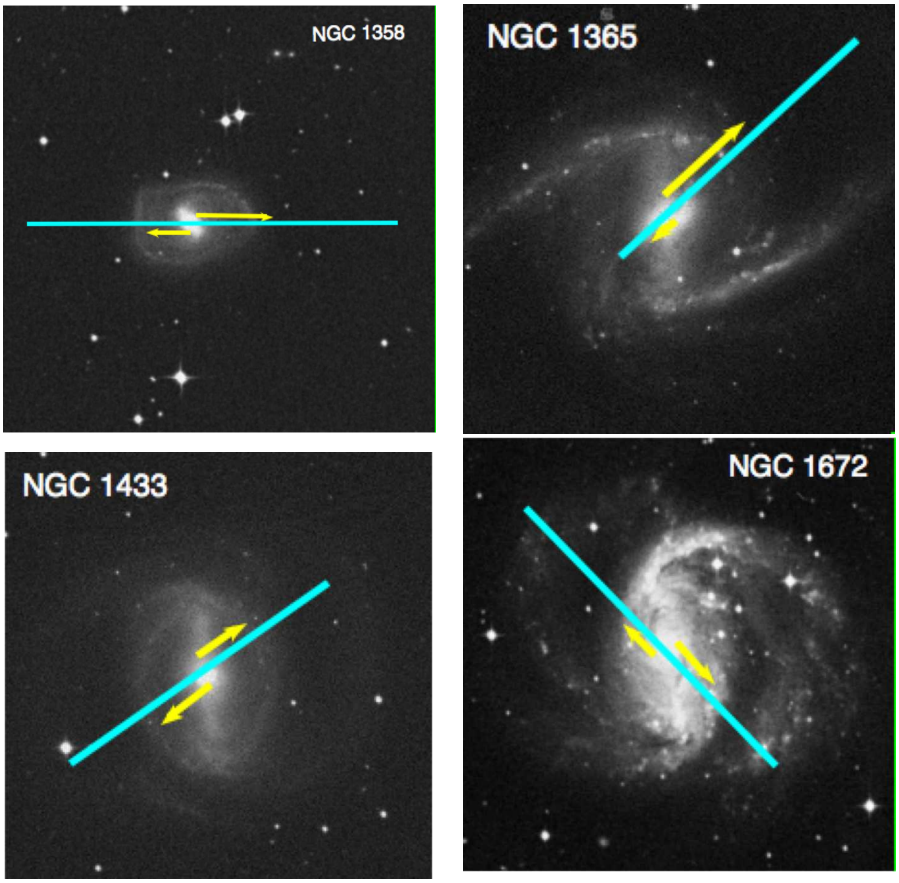

Figure 1. Observational setup for our sample of galaxies. The images all cover an area of 450×450″. The yellow arrows indicate the extent of the stellar population gradients presented here.

fit allows for a low-order Legendre polynomial in order to account for small differences in the continuum shape between the pixel spectra and the templates. The best fitting template mix is determined by a χ^2 minimization in pixel space. Emission line spectra at each radius were substracted from the observed spectra for the subsequent analysis. Figure 2 shows the central spectrum of NGC 1365 before and after subtracting the emission spectra. Figure 3 shows the line-of-sight velocity and the σ of the stellar and gaseous components as a function of radius for our sample of galaxies. We fit the position and the σ of each atomic species independently. Sarzi et al. (2006) caution `GANDALF` users about this procedure when emission lines cannot be measured confidently, as contamination due to template mistmatch can still be important and result in spurious detections. This problem affects the Hβ line, which we cannot measure in all spectra because it does fall in the gap of the detector. Furthermore, spurious detections would result in velocities that differ from those measured with other lines and, in our case, the velocities measured with all the emission lines are very consistent (see § 3.3), giving support to our approach of fitting all the lines independently.

The errors in the radial velocity and velocity dispersion were computed through numerical simulation. In each simulation, a bootstrapped galaxy spectrum, obtained using the error spectrum (see § 2), was fed into the algorithm (a

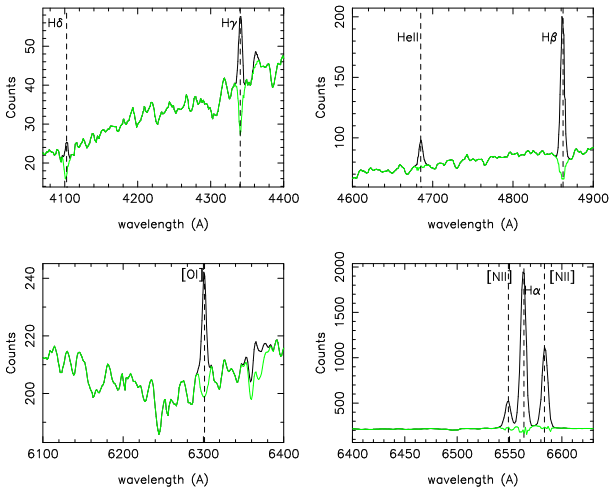

Figure 2. Central spectrum of NGC 1365 before (black line) and after (green line) subtracting the emission spectra using `GANDALF`.

different optimal template is computed in each simulation). Errors in the final parameters were computed as the unbiased standard deviation of the different solutions. The final errors are expected to be quite realistic, as they incorporate all the uncertainties of the entire reduction process, from the first steps (e.g., flat fielding) to the final measurements of the parameters. We did not attempt to correct the velocities for inclination, as this correction is very uncertain and very large for nearly face-on galaxies.

3.1 Reliability of the derived σ

Given the resolution of our data $\sigma_{\rm inst} \sim 90$ kms^{-1}, it is worth testing if the derived velocity dispersions (in some cases around $\sim$50 kms^{-1} are reliable. For this reason we perform a series of simulations using synthetic spectra corresponding to different star formation histories, trying to mimic as far as possible the real data. In particular, we took the parametrized star formation histories given as examples in the MILES webpage (`http://www.iac.es`) that include exponential, constant and composition of different burst with metallicities ranging from $[Z/H] = -2.32$ to 0.22. We first broadened the synthetic spectra to the nominal instrumental resolution of our data by convolving with a Gaussian broadening function and then we broadened again those spectra with velocity dispersions from 50 to 120 kms^{-1} in steps of 10 kms^{-1}. Afterwards, we added noise to simulate the signal-to-noise of the observed spectra (S/N(Å)$\sim$50 which is the minimum we used to bin our data). The velocity dispersion was then measured using `ppxf` using the same parameters as we used for the real data. The results are plotted in Fig. 5. As can be seen, we do not detect any significant systematic effect between the input and output velocity dispersions. A similar result was found by Toloba et al. (2011) using a different code. In particular, these authors found that for S/N(Å)>50, the relative error in the derived σ was always lower than 10% for σ down to half the instrumental resolution.

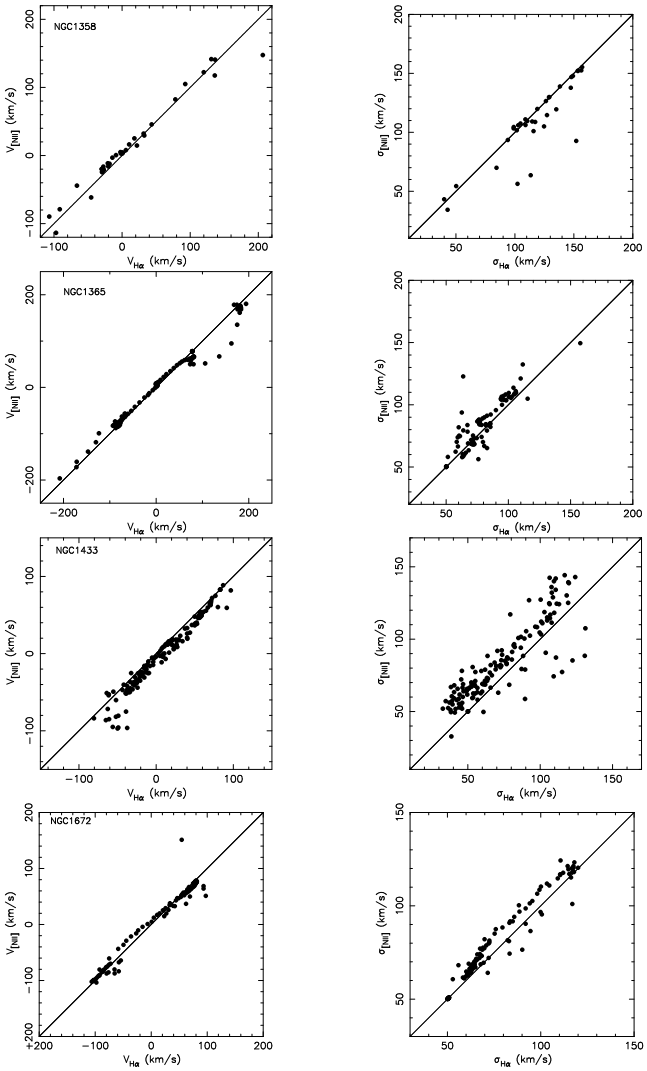

Figure 4. Comparison of the radial velocity and velocity dispersion of the emission lines Hα and [NII] measured with `GANDALF`.

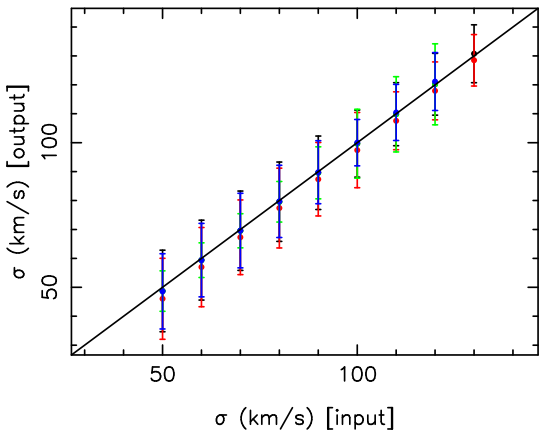

Figure 5. Comparison of the input vs. calculated velocity dispersion in a series of simulations performed in synthetic spectra with different values of metallicities and corresponding to different star formation histories (see text for details). The solid lines indicate the 1:1 relation.

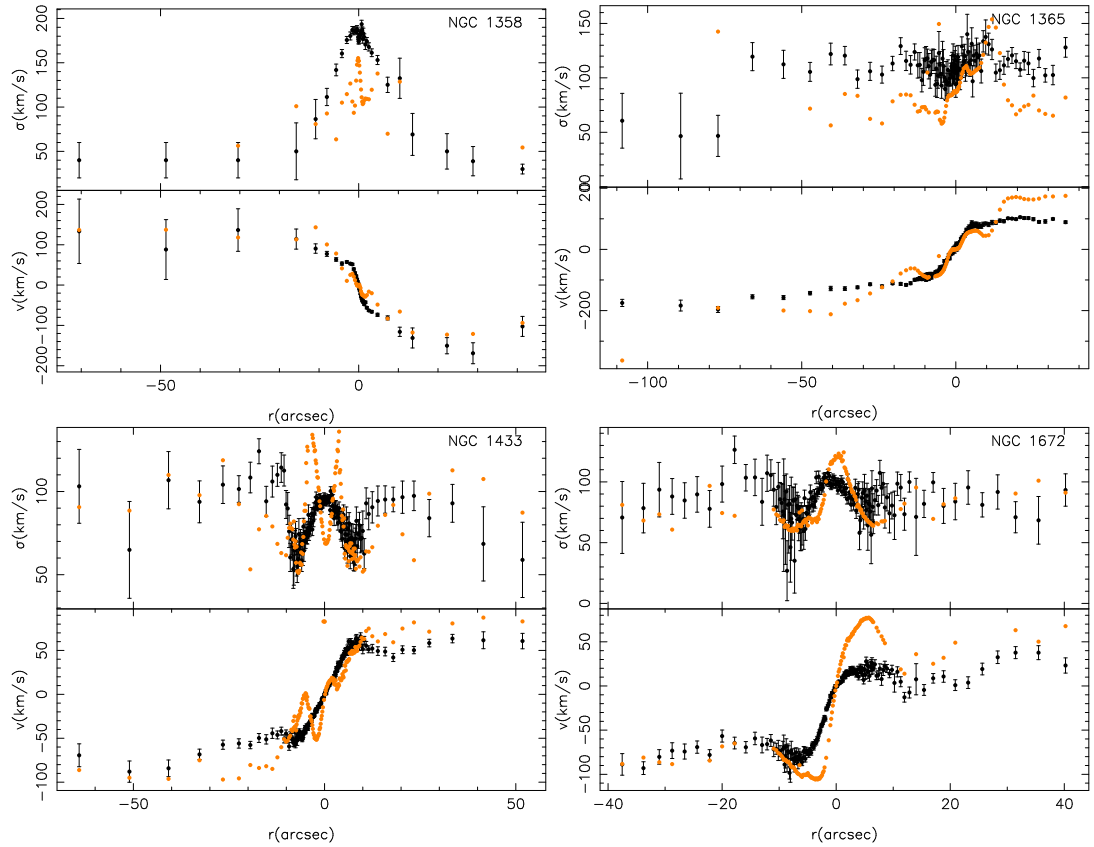

Figure 3. Line-of-sight velocity as a function of radius and velocity dispersion for the stellar component (black points) and the gaseous components (colored points). The kinematics for the gas component has been measured using different emission lines as indicated in the insets.

3.2 Stellar Radial Velocities and Velocity Dispersion

All our galaxies show clear rotation, while the σ profiles behave quite differently. The σ variations with radius are very small for NGC 1672 and NGC 1365, as found in previous studies (Ganda et al. 2006; Pérez et al. 2009) for late-type spirals. For the early-type spirals NGC 1358 (S0) and NGC 1433 (Sab), the velocity dispersion profiles decline with increasing radius, as has been found in many elliptical galaxies (e.g., D'Onofrio et al. 1995; Sánchez-Blázquez et al. 2006). The galaxy NGC 1433 has a very strong local minimum in the velocity dispersion at the position of the ring (Buta et al. 2007), indicating the colder nature of this structure, but then the trend of σ is to decrease towards the external regions, as in NGC 1358.

In Pérez et al. (2009), we found that *all* early-type spirals with bars show disc-like structures in their centres, inferred from their kinematics. These structures are characterised by a central velocity dispersion minimum (σ-drops), central σ plateaus, and/or a clear rotating inner disc or ring, as derived by the line-of-sight position-velocity diagram. For the present sample, a σ-drop is present in the early-type spiral NGC 1365.

3.3 Gas Velocities and Velocity Dispersion

The kinematics of the gaseous component have been derived using different emission lines. In principle, the Hα emission could be dominated by gas with different kinematics than that contributing to the [NII] emission. However, we do not find any significant difference, neither in the line-of-sight velocity nor in the velocity dispersion measured for different emission lines, whether it is Hα or [NII] (see Fig. 4). Gas always rotates faster and shows structures like wiggles (see also Ganda et al. 2006). Deviations from circular motions (most likely caused by the bar) are clearly evident in all the curves, while the radial velocities of the stellar components are much smoother.

4 STAR FORMATION HISTORIES

Disc galaxies are obviously composite systems in which several generations of stars contribute to the integrated light spectrum. While for spheroidal systems, single stellar populations are, in many cases, not a bad approximation of the star formation history, for disc galaxies this is certainly not true. In the last few years, new models of stellar populations have been developed which predict not only the strength of individual characteristics, but the entire spectral energy distribution for a population of a given age and metallicity (e.g. Vazdekis 1999; Bruzual & Charlot 2003, BC03 hereafter; PEGASE-HR (LeBorgne et al. 2004), Coelho et al. 2007;

Vazdekis et al. 2010). This has led to the parallel development of numerical techniques to derive the star formation history of galaxies using as much information as possible from the spectra (Heavens et al. 2000; Panter et al. 2003; Cid Fernandes et al. 2005; Ocvirk et al. 2006ab; Tojeiro et al. 2007; Koleva et. 2009).

We use here `STECKMAP` (STEllar Content and Kinematics via Maximum a Posteriori, Ocvirk et al. 2006a,b), along with 2 sequences of stellar population models taken from Bruzual & Charlot (2003) and Vazdekis et al. (2010), spanning an age range $10^8 - 1.7.10^{10}$ yr divided in 30 logarithmic age bins, and a metallicity range [Z/H]=[+0.2, -1.3]. `STECKMAP` is a Bayesian method that simultaneously recovers the kinematic and stellar population properties via a maximum *a posteriori* algorithm. It has been extensively tested and used in a variety of applications, ranging from globular clusters (Sharina & Davoust 2008; Ocvirk 2010) to stripped galaxies (Pappalardo et al. 2010). It is a public tool and can be obtained at `http://astro.u-strasbg.fr/~ocvirk/`. We note also that an online service has been recently launched, allowing the user to submit their spectrum, run the code on the remote server, and collect the results. The latter can be accessed at `http://astar.aip.de:20202/steckmap`. The method is not parametric and does not make any *a priori* assumption regarding the star formation history. The only condition that `STECKMAP` imposes is that the different unknowns, namely the stellar age distribution (hereafter, LIGHT), the age-metallicity relation (hereafter, AMR), the line-of-sight velocity distribution (LOSVD) or the broadening function (hereafter, BF), have to be smooth in order to avoid extreme oscillating solutions that are not robust and most likely unphysical. The objective function, i.e., the function to minimise, is defined as:

$$Q\mu = \chi^2(\mathbf{s}(\mathbf{x},\mathbf{Z},\mathbf{g})) + P_\mu(\mathbf{x},\mathbf{Z},\mathbf{g}), \quad (1)$$

which is a penalised χ^2, where $\mathbf{s}$ is the model spectrum resulting from the LIGHT $\mathbf{x}$, the AMR $\mathbf{Z}$, and the BF $\mathbf{g}$. The penalisation P_μ can be written as: $P_\mu(\mathbf{x},\mathbf{Z},\mathbf{g}) = \mu_\mathbf{x} P(\mathbf{x}) + \mu_\mathbf{Z} P(\mathbf{Z}) + \mu_\mathrm{v} P(\mathbf{g})$, where the function P gives high values for solutions with strong oscillations (ie. LIGHT and AMR changing rapidly with time or noisy BF) and small values for smoothly varying solutions. As explained in Ocvirk et al. (2006a), adding the penalisation P to the objective function is exactly equivalent to injecting *a priori* information into the problem. In practice, this is like imposing an *a priori* probability density to the solution as $f_\mathrm{prior}(\mathbf{x}) = \exp(-\mu_\mathbf{x} P(\mathbf{x}))$ (see Ocvirk et al. 2006 for more details).

For this work, we define P as a quadratic function of the unknown $\mathbf{x}$, involving a kernel $\mathbf{L}$, as in Eq. (29) of Ocvirk et al. (2006a):

$$P(\mathbf{x}) = \mathbf{x}^\top \cdot \mathbf{L}^\top \cdot \mathbf{L} \cdot \mathbf{x}. \quad (2)$$

We use a Laplacian smooting kernel for the LIGHT and BF (i.e. $\mathbf{L} = \mathbf{D_2}$), and a gradient kernel for the AMR (i.e. $\mathbf{L} = \mathbf{D_1}$), as in Ocvirk (2010), using the definitions of Ocvirk et al. (2006a).

Choosing the right values of the smoothing parameters $\mu_{\mathbf{x},\mathbf{Z},\mathrm{v}}$ is not a trivial problem. In principle, one could choose the values giving the smaller χ^2 in the fit, but this usually yields a wide range of smoothing parameters, spanning typically 3-4 decades, in which the fit is acceptable. Although this affects the detailed shape of the LIGHT, AMR and BF, it does not impact the overall interpretation of the fit, and we checked via Monte Carlo simulations that the global shape of the solutions, and in particular the integrated quantities such as luminosity and mass-weighted ages and metallicities are stable for this range of smoothing parameters. The final chosen values were $\mu_\mathbf{z} = 10^2$ and $\mu_\mathbf{x} = 1$.

For this work, we have not fit simultaneously the star formation histories and the kinematics, and we use the values obtained with `ppxf`. The reasons are explained in detail in Appendix B. Basically, the existing degeneracy between the metallicity and the velocity dispersion (Koleva et al. 2007) biases the mean-weighted metallicites if both parameters are fitted at the same time. We found that this degeneracy affects mostly the mass-weighted values of the metallicity (see Appendix), in the sense that the derived mass-weighted metallicity values are higher if the kinematics are not fixed.

Error bars were calculated by means of Monte Carlo simulations where each pixel is perturbed randomly according to the error spectrum, and assuming a Gaussian distribution. However, the errors calculated in this manner are very small, due to the high signal-to-noise ratio of our data. For this high S/N data, the errors in the theoretical models have usually a stronger impact on the solution (Ocvirk et al. 2006a). Several studies have now compared the results in the star formation histories recovered using different models (Koleva et al. 2008; Coelho, Mendes de Oliveira & Cid Fernandes 2009; González 2009 & Cid Fernandes 2010). In particular, Koleva et al. (2008) found that the success in the recovery of the age and metallicity of a single synthetic population depends critically on the atmospheric parameter coverage of the stellar library used in the SSP models. They found that results using MILES and PEGASE-HR are very consistent for ages larger than 1 Gyr and [Z/H] > -1, while the results using BC03 differ at metallicities far from solar.

For this reason, we make use of several different stellar population models and check the consistency of our results to this choice. We employ both the new stellar population models by Vazdekis et al. (2010, V10 hereafter) that include the new and improved stellar library MILES (Sánchez-Blázquez et al. 2006; Cenarro et al. 2007 and Bruzual & Charlot (2003, BC03 hereafter).

In order to deal with possible flux calibration errors, we multiply the model by a smooth non-parametric transmission curve, representing the instrumental response multiplied by the interstellar extinction. This curve has 30 nodes spread uniformally along the wavelength range, and the transmission curve is obtained by spline-interpolating between the nodes. The latter are treated as additional parameters and adjusted during the minimisation procedure. This continuum matching technique is similar in essence to the multiplicative polynomial used by `NBursts` (Chillingarian et al. 2007) or `ULySS` (Koleva et al. 2009b). It has also been successfully used by Ocvirk (2010) and will be detailed in a forthcoming paper.

We fit the wavelength range $\lambda\lambda$4150-6100 Å masking the regions corresponding to the detector gaps and masking other regions where the spectrum was affected by sky residuals. In some cases, the TiO molecular band was also masked, as the models did not seem to fit it properly. Figure 6 shows the central spectrum of the four galaxies analysed in this

study, together with the best fit obtained by STECKMAP using the V10 stellar population models. The underlying continuum shape has been removed from both the model and the data.

One of the most important problems affecting the stellar population studies is the well-known age-metallicity degeneracy, i.e., the colours and spectral characteristics of a given population can be mimic with another population younger but more metal rich or older but more metal poor. To see the extent by which the results obtained with steckmap are affected by this degeneracy we use a 10 Gyr and a 1 Gyr solar metallicity SSP from Vazdekis et al. (2010) and added noise to obtain a spectrum with a signal-to-noise per Å of 50. Then we performed 50 Montecarlo simulations in which each pixel was perturbed with the associated noise error, following a Gaussian distribution. For each simulation a new value of the age and metallicity was derived using three different techniques: (1) spectral fitting with steckmap; (2) classical index-index diagram fit (using [MgbFe]-Hβ diagram) and (3) multi-index fitting technique (following Proctor & Sansom 2002). The techniques (2) and (3) have been extensively used by several authors to derive their stellar population SSP-equivalent parameters (e.g., Trager et al. 2000; Kuntschner et al. 2006; Sánchez-Blázquez et al. 2006, 2007; Paudel et al. 2010, among many others). The results are displayed in Fig 7. It can be seen that the age-metallicity degeneracy is very much reduced using steckmap compared with the other two widely-used techniques.

5 RESULTS

5.1 Stellar Population Gradients

Figure 8 shows some examples of the derived flux fraction contributions of stars in the various age bins at different radii for our sample of galaxies using both sets of models, V10 and BC03. In general, the star formation histories that we obtain are compatible with being exponentially declining with timescales τ between 2 and 7 Gyr. Secondary bursts of star formation are seen at several radii within the sample.

To quantify the gradients in a way that can be compared with theoretical predictions, Figs 9 and 10 show the mass- and luminosity-weighted metallicities and ages as a function of radius for our sample of galaxies obtained with V10 stellar population models. The mass- and luminosity-weighted quantities are obtained respectively as:

$$\langle q \rangle_{\rm MW} = \frac{\sum_i {\rm MASS}(i) \log q_i}{\sum_i {\rm MASS}(i)}, \qquad \langle q \rangle_{\rm LW} = \frac{\sum_i {\rm LIGHT}(i) \log q_i}{\sum_i {\rm LIGHT}(i)}, \tag{3}$$

where q is the physical parameter we want to estimate, i.e., age or metallicity, and MASS(i) and LIGHT(i) are respectively the reconstructed mass and flux contributions of the stars in the i-th age bin, as returned by STECKMAP. We have chosen here to weight both the ages and metallicities in a base-10 logarithmic scale, as these values are more similar to the SSP-equivalent parameters (see Sec /refsec:ssp). The mean values would have changed if, instead, linear averages were computed. As an example we plot in Fig. 11 the mass- and luminosity-weighted age and metallicities for NGC 1433

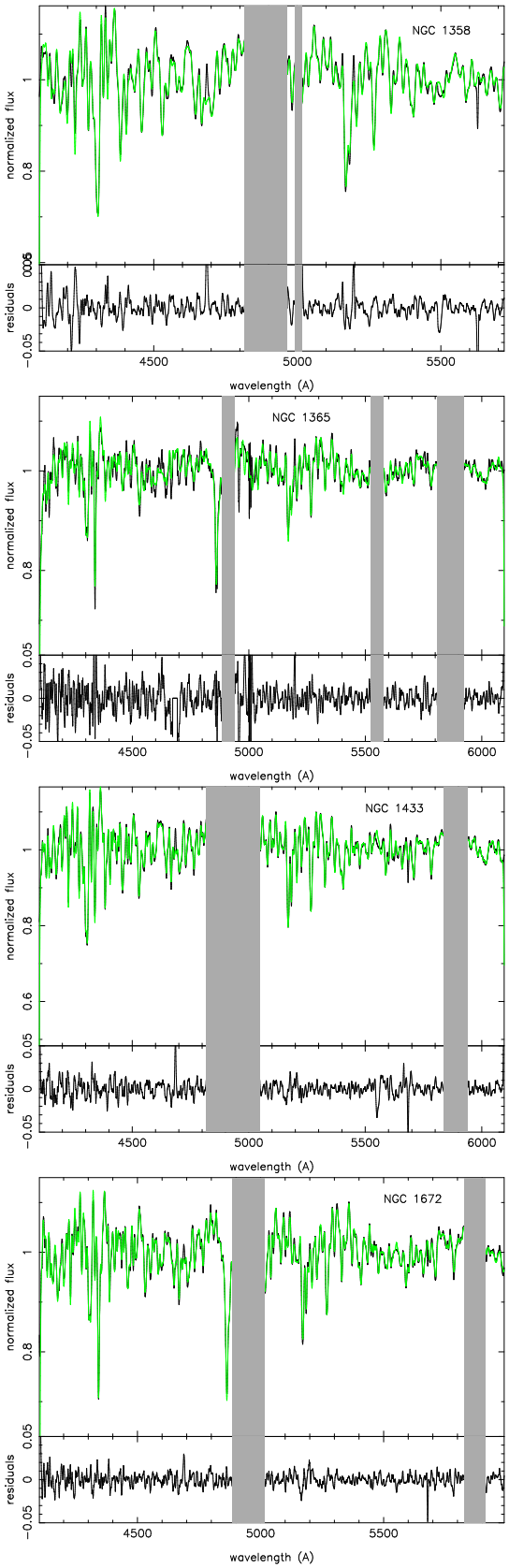

Figure 6. Central spectrum of the galaxies (black line) with the best fit obtained by STECKMAP (green line). The grey areas show the masked parts of the spectra: two of them correspond to the gap of the detectors while others mask areas of the spectrum affected by sky residuals.

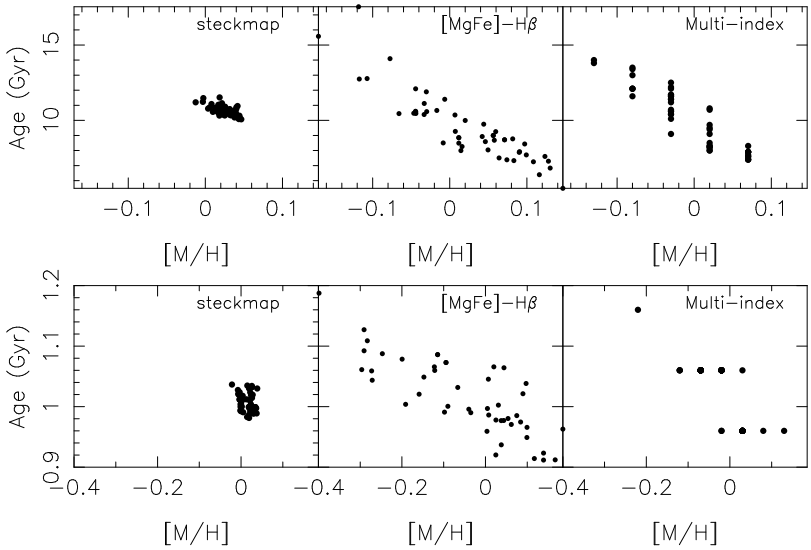

Figure 7. Measured age-metallicity using three different techniques (as indicated in the labels), on two synthetic spectra with ages 1 (bottom panel) and 10 Gyr (upper panel) and solar metallicity, perturbed with Gaussian noise expected for a spectrum with a S/N(Å) 50.

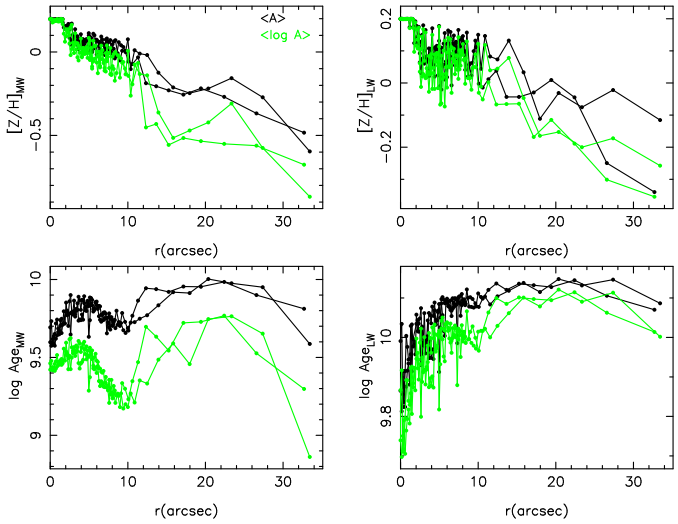

Figure 11. Comparison of the mass- and luminosity-weighted age and metallicity for NGC1433 when the means are performed using a logarithmic scale (green line) and using a linear scale (i.e. log removed in Eq. 3, black line).

comparing the values when instead of log(age) and [Z/H], Z and age are averaged. As can be seen, there can be important differences in the weighted values of age and metallicity depending on how the mean is computed. It is important then, to specify the way in which the average is calculated.

We explore, in appendix A if these gradients are model dependent. We found that for populations younger than ∼3 Gyr[3], metallicities with BC03 tend to be lower and the ages higher than those derived with V10. For the rest of the populations, the mean age and metallicity values are not dependent of the model used. In our sample of galaxies, significant differences are only visible in the bulge region of NGC 1433 and the ring region in NGC 1672. In the figures, we indicate the position of the effective radius of the bulge and the scale-length of the discs (see Table 1). We now analyse the populations in these two regions separately.

[3] We have not explored the whole parameter space because we are limited by the values measured in our sample and, therefore, we cannot provide with a range of ages and metallicites where the models agree or disagree as done, e.g., in Koleva et al. (2008)

5.2 Bulge Region

The stellar population parameter profiles in the bulge regions show a variety of behaviour. The luminosity-weighted metallicity profile decreases in 3 of the 4 galaxies but increases in NGC 1365. The luminosity-weighted age profile in the bulge region also behaves differently depending on the galaxy, with profiles that do not always increase or decrease monotonically. The luminosity-weighted age reflects the presence of dynamically cold structures, where there has been (or where there is currently) recent star formation, manifesting itself as central discs (e.g. in NGC 1433) or rings (NGC 1365 and NGC 1433 at r∼7 and 10 arcsec respectively, and NGC 1672 at r∼ 9 arcsec). The mass-weighted values are much flatter, indicating that the bulge regions are dominated in mass by an old stellar population (10-15 Gyr), although the central discs in NGC 1672 and NGC 1433 show mass-weighted ages slightly younger (∼6 Gyr). Very similar conclusions were reached by MacArthur et al. (2009) in their larger sample of galaxies, where also a large variety of age and metallicity gradients were found while the mass-weighted ages were always old.

Curiously, NGC 1365 shows a much lower metallicity in the bulge region than the other galaxies of our sample. NGC 1365 is an Sb galaxy with a star formation history that can be reproduced with an exponentially declining function with $\tau \sim 6$ Gyr at all radii within the bulge region except in the nuclear ring (radius $\sim$ 7 arcsec) where there is current star formation. The most puzzling aspect is that the gas phase metallicity of this galaxy is quite high in this region, $\sim 12 + \log O/H = 9.15$ (Roy & Wash 1997; Pilyugin, Contini & Vilchez 2004). Furthermore, contrasting the low stel-

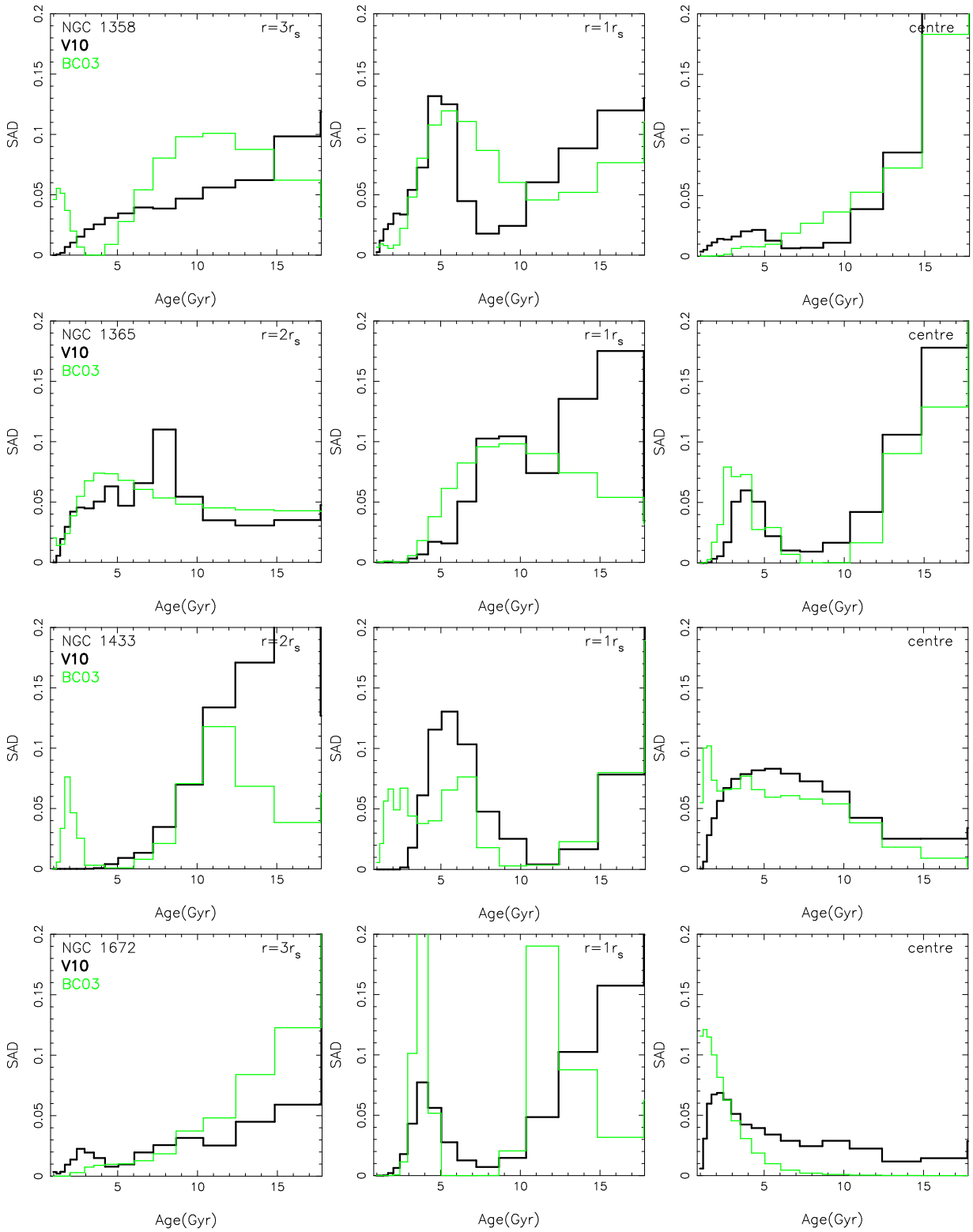

Figure 8. Stellar flux fractions at different ages calculated at different scalelengths of the disc. Black lines indicate the results obtained when the V10 models are used while in green we have plotted the results obtained with the B03 models.

lar stellar metallicity values in the bulge region, this galaxy has the largest metallicity of the sample in the disc region (see next Section and Fig. 10). One possibility is that the metal poor stellar population in the center formed from low-metallicity gas that could have been both, accreted or driven from the external parts of the galaxy to the circumnuclear region by the bar. Subsequently, the newly formed stars enriched the interestellar medium to the levels we observe now. To reach the level of enrichment that is observed, the star formation had to be rather intense. It has been suggested

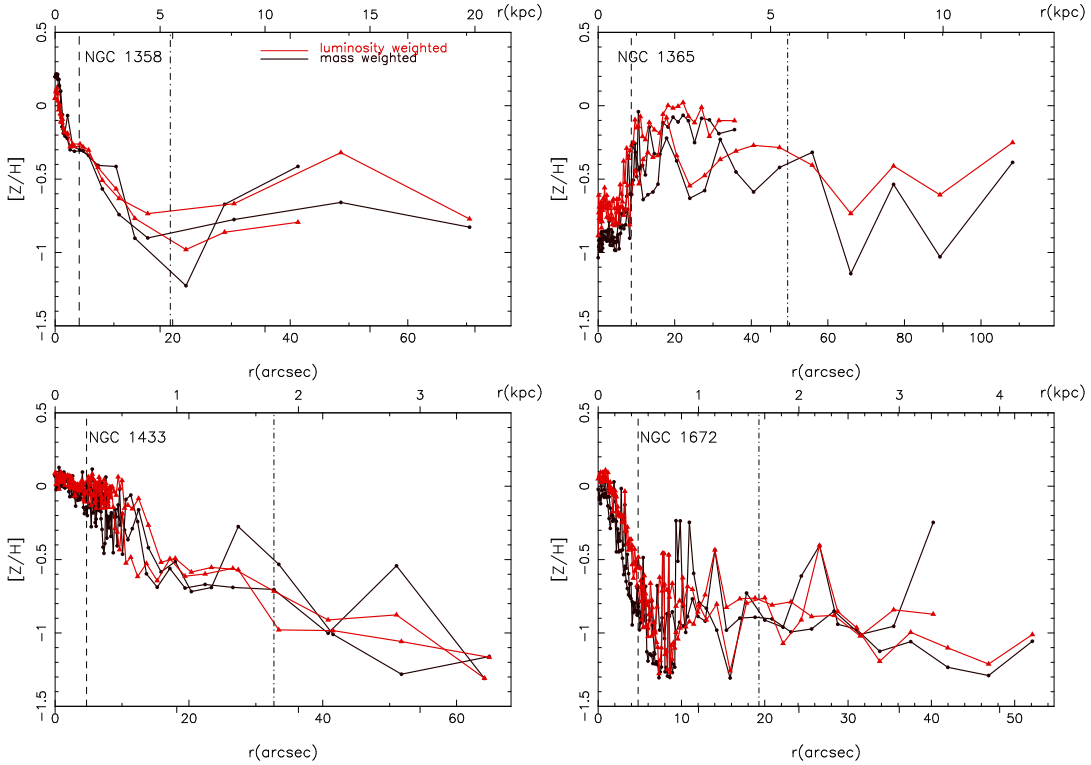

Figure 9. Mass- and luminosity-weighted metallicity gradients derived from the recovered star formation history using V10 models. Vertical dashed lines indicate the position of the effective radius of the bulge while dot-dashed lines show the disc scale-length, obtained from the references indicated in Table 1.

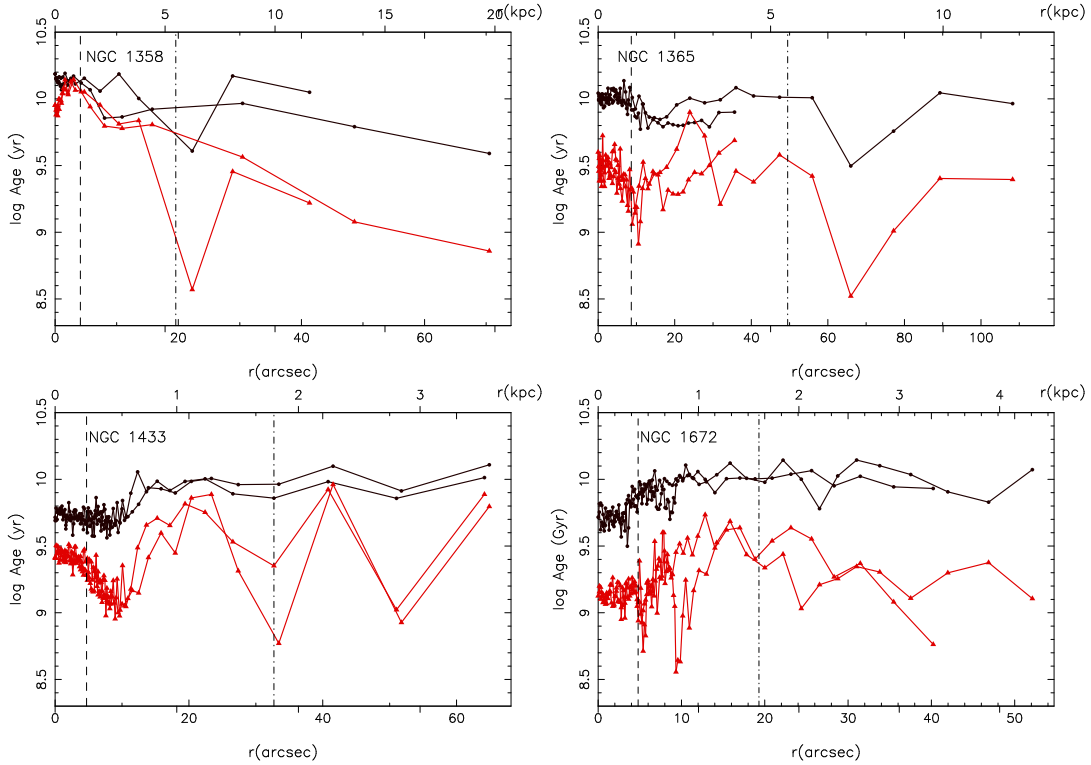

Figure 10. Mass- and luminosity-weighted age gradients derived from the recovered star formation history. The meaning of the colors and symbols are the same as in Fig. 9

that NGC 1365 has recently ($\sim$ 1 Gyr ago) experienced an interaction that made the disc unstable, producing the development of a bar (Zanmar-Sánchez et al. 2007). Inverse metallicity gradients in the central parts of merger remnants has been observed in the other galaxies in the local Universe (Rupke et al. 2010; Kewley et al. 2010).

5.3 Disc Region

In general, the inner disc region of all the galaxies (as in the bulge region) is dominated by an old population (see Fig. 10). The mass-weighted age gradients in the disc region are always quite flat with a mean age around 10-12 Gyr. The luminosity-weighted age gradient is either flat or slightly negative (at 2 scalelengths, the age decrease is 4 Gyr for NGC 1672 and $\sim$4.7 Gyr for NGC 1358) consistent with an inside-out formation of the disc.

The mass- and luminosity-weighted metallicity gradients show very similar slopes (see Fig. 9), suggesting very little evolution with time in the gradients of our galaxies.

An aside needs to be made here: as we mention in Sec. 4, the stellar population parameters have been calculated fixing the kinematics to the values obtained with `GANDALF`. We have noticed that when this is not done, a degeneracy between the σ and metallicity appears, producing a systematic effect for which luminosity weighted values are lower than the mass-weighted ones (see Appendix B). This is true using both, `STARLIGHT` and `STECKMAP`. This effect is also visible in some of the gradients shown by MacArthur et al. (2009). We speculate that their mass-weighted metallicities can be also biased due to this degeneracy.

5.4 Comparison Between the Disk and the Bar Regions

Bars are very important structures that can influence the evolution of disc galaxies enormously. However, little is known about their own destiny. In particular, for our study, it is important to know if they can survive for a long time or whether they are easily destroyed. There is still no consensus in the literature about this point (Bournaud & Combes 2005; Shen & Sellwood 2004; Berentzen et al. 2007). If bars are not long-lasting structures, the fact that a galaxy does not have a bar now, does not mean that it did not have it in the recent past. In this case, the lack of differences in the stellar gradients would not mean that the bar did not have an influence on producing radial mixing.

Two of the galaxies of the sample presented here, NGC 1358 and NGC 1433 were studied by Pérez et al. (2009). There, we presented long slit spectroscopy along the bar of the galaxies, finding three different types of bars according to their age and metallicity distribution as a function of radius: (1) Bars with young/intermediate age and negative metallicity gradients. These bars are present in galaxies with the lowest velocity dispersion in our sample; (2) Bars with zero metallicity gradient and younger stellar populations at the end of the bars; and (3) Bars with old stellar populations and positive metallicity gradients. This type was found predominantly in those galaxies with a higher central velocity dispersion. NGC 1358 belongs to the third group while NGC 1433 is part of the second. One of the results from that study was that the majority of the bars in our sample (biased towards morphologically classified early-type spirals and S0) were composed of old stellar populations. However, the fact that the bars have old ages does not mean, necessarily, that the structure is old, as the bar might have been formed, recently, out of old stars in the disc. One way to disentangle these two options is comparing the stellar population of the disc and the bar. In Pérez et al. (2009) we performed the analysis by comparing line-strength indices with SSP models. There, we used the data to perform an analysis similar to the one presented here and ran `STECKMAP` on the spectra as a function of bar radius. Figure 15 shows the comparison of the luminosity-weighted age and metallicity along the disc and the bar. As can be seen in the two studied galaxies, the stars in the bar are older and more metal rich than those of the disc. Furthermore, the gradient in both parameters is much flatter in the bar. In general, the stellar content of the bar is more similar to that of the bulge than to the disc. This confirms that, at least for some galaxies, the bars are, in fact, long-lasting structures. The two galaxies for which we have been able to perform the comparison are very early-types. It will be interesting to perform this comparison for more late-type spirals, as there must be a correlation between the age of the bars and the morphological type of the galaxy (e.g., Gadotti 2008).

6 LINE-STRENGTH INDICES AND SINGLE STELLAR POPULATIONS

Most of the studies of unresolved stellar populations have not derived whole star formation histories, but SSP-equivalent ages and metallicities using combinations of line-strength indices, most commonly Lick/IDS indices (Trager et al. 2000a; Sánchez-Blázquez et al. 2006b; Ganda et al. 2007). This approach has the advantage that it allows one to derive not only average ages and metallicities, but also to obtain an estimation of the relative chemical abundance ratios, as the sensitivity of individual Lick indices to the abundance of different chemical species is different and has been calibrated by different authors (Tripicco & Bell 1995; Korn, Maraston & Thomas 2005; Houdashelt, Trager & Worthey 2005). New models that predict the whole spectra for populations with different chemical composition are being built now (e.g., Coehlo et al. 2009; Lee et al. 2009) and, in the future, it will be posible to derive this information also from full spectral fitting. The index analysis has the disadvantage that higher signal-to-noise ratio is needed and, also, that if the sensitivity of the indices to changes in the chemical abundances of different elements is not properly calibrated, the results might be biased depending on the indicator used to perform the analysis (more than with the full spectral fitting). Furthermore, the comparison of indices with SSP-models can only give us SSP-equivalent parameters and those are degenerate to different star formation histories. In this section, we derive SSP-equivalent ages, metallicities and α/Fe ratios by comparing Lick/IDS indices to the new models of V10 in order to compare these values with the luminosity- and mass-weighted values derived in Sec. 5.1.

The canonical models of V10 were built using an empirical stellar library (MILES, Sánchez-Blázquez et al. 2006) with chemical abundance ratios matching those of the solar

neighbourhood and with isochrones assuming a solar partition for the different elements. Because we want to derive not only global metallicities, but also chemical abundance ratios, we modified the predictions for individual indices for different patterns of chemical abundances. Following the approach of several previous authors (e.g., Tantalo, Chiosi & Bressan 1998; Trager et al. 2000a; Thomas, Maraston & Bender 2003; Sánchez-Blázquez et al. 2009b), we did not change the different elements individually but assumed that some of them are linked nucleosynthetically and, therefore, vary in lock-step. We group the different elements in enhanced (E hereafter), including N, Ne, Na, Mg, C, Si and S (i.e., most α-elements released in Type II SN plus N and C); depressed, including Ca and Fe, and unchanged (the rest), in such a way that the global metallicity of the models remains unchanged. We developed models with enhancements from [E/Fe]=−0.1 to 0.5 in steps of 0.05. In all cases, C is enhanced only half the amount of the other enhanced elements. The reason for that is that enhancements of the order of ∼0.3 dex bring the C/O ratio very close to the values at which a carbon star is formed (see Houdsashelt et al. 2002; Korn et al. 2005). The response functions by Korn et al. (2005) are calculated for variations in the abundances of different elements of 0.3 dex. The responses for different enhancements different from 0.3 dex were obtained using the procedures described in Sánchez-Blázquez et al. (2009b) (originally described by Trager et al. 2000).

We derived SSP-equivalent parameters age, [Fe/H] and α/Fe-abundance ratios for all the galaxies of the sample using the χ^2 minimization technique detailed in Proctor & Sansom (2002) and Proctor et al. (2004ab). The technique involves the comparison of as many indices as possible to simple stellar population models. We find that it is extremely difficult to fit simultaneously all the indices with a single stellar population, most likely because the star formation histories of our sample cannot be approximated by an SSP. After several tests we decided to avoid the bluest region of the spectra (the Hδ indices and the CN) because they deviated the most in all the fitted spectra. These indices are more sensitive to the presence of young populations than the rest of the Lick indices and, therefore, removing them from the fit we are biasing our equivalent ages toward older values. Contrary to what was done in Proctor et al. (2004ab) we did use the same indices to fit all the spectra. This is because different indices are sensitive to different populations and different chemical species so if the galaxies do not share the same chemical abundance patterns as the models we are using, the results can be biased by using different sets of indices at different radius. Furthermore, the use of different indicators to obtain SSP-equivalent parameters will give different results in case the star formation history is not a single burst (Sánchez-Blázquez et al. 2006b; Schiavon et al. 2007). For these reasons, all the indices that in some of the galaxies of our sample fell in the gaps of the detectors were eliminated from the fit. In total, we use 10 Lick/IDS indices (ie., all the Lick/IDS indices that our spectral range allowed us to measure excluding those that fell in the gaps of the detector).

Residuals from the best-fitting (observed value minus best fitting value expressed in terms of the index errors) indices for all the galaxies are summarised in Fig. 12. The points represent the average deviation from the best-fitting values while the error bars show the RMS for all the points as a function of radius. As can be seen, for the set of the indices that we have used, the mean differences between the fitted and the measured indices are very small. This indicates that despite that fact that the stellar populations of disc galaxies cannot be reproduced by a single burst, most of the Lick indices are sensitive to the same stellar populations once the bluest indices are excluded.

Figure 13 shows the derived age, [Z/H] and [E/Fe] profiles for our sample of galaxies. The shape of the profiles is more similar to the luminosity-weighted than to the mass-weighted values derived in the Sec. 4, as expected. However, the SSP-equivalent ages are, in general, younger. This is in agreement with the results of Serra & Trager (2007) who compared the SSP-equivalent ages and metallicities with the V-band luminosity weighted ones (not exactly the same as the one derive here) using artificial star formation histories of two instantaneous bursts. Figure 13 also shows the mean linear-weighted values compared with the log-weighted values. It can be seen that the log-weighted values are more similar to the SSP-values, with a trend for the linear weighted ages to be larger, as expected.

Figure 14 shows a 1:1 comparison between the SSP-equivalent ages and metallicities and the luminosity and weighted- values for the different galaxies. As can be seen, luminosity-weighted values and SSP-equivalent values tend to agree for old ages and high metallicities. As the ages get lower, SSP-equivalent values are systematically smaller than the luminosity-weighted and the same trend is observed for metallicities. Mass-weighted ages, on the contrary are always higher than the SSP-equivalent ones and much more constant, reflecting what we mentioned before, that the galaxies are dominated in mass by an old stellar population, independently of radius. The mass-weighted metallicity, however, follows a similar trend than the luminosity-weighted one and, in the same way, agrees with the SSP-equivalent one for high metallicity-values.

Several authors have analysed stellar populations of bulges using line-strength indices and derived SSP-equivalent stellar population parameters (e.g., Trager, Dalcanton & Weiner 1999; Goudfrooij, Gorgas & Jablonka 1999, Proctor & Sansom 2002, Falcón-Barroso, Peletier & Balcells 2002; Morelli et al., Thomas & Davies 2006, Moorthy & Holztman 2006; Peletier et al. 2007). Some of them have presented gradients as a function of radius. In general, it is found that bulges of galaxies have negative metallicity gradients (~ -0.2 dex), positive age gradients (younger in the center) of ∼3-5 Gyr per decade of variation in radius, and null or slightly positive [E/Fe] gradients (Jablonka et al. 2007; Morelli et al. 2006). Moorthy & Holtman (2006) found that if positive age gradients (central regions being younger) were found, they were invariably in barred galaxies, although barred galaxies could also show negative gradients. Jablonka et al. (2007), however, found that for most galaxies of their sample, the age gradient was positive –albeit always very small and, in many cases, compatible with being null– independently of them being barred-or not barred. In fact, Jablonka et al. (2007) did not find any difference between the stellar populations (SSP-equivalent parameters) of barred and non-barred galaxies. The differences between Jablonka et al. and Moorthy et al. studies can be due to the fact that Jablonka et al. (2007) observed edge-on galaxies and, there-

fore, avoided the contribution of disc-like components such as bars, rings or nuclear discs. The results of Morelli et al. (2007) are consistent with Jablonka et al. (2007), despite the fact that their galaxies are face-on. However, their sample is composed of non-barred (or very weakly barred) galaxies and this limits the number of subcomponents, such as rings and nuclear discs, present in the sample[4]. Furthermore, the sample is biased towards early-type systems.

We also found a variety of age gradients depending on the galaxy, ranging from flat (NGC 1365), to positive (NGC 1672), to negative (NGC 1433) and an equivalent behaviour in the metallicity gradient. We found that the variety of gradients in our galaxies is due to the contrast produced by the presence of different components, such as rings and nuclear discs. As mentioned in Sec. 5.1, NGC 1365 presents a much lower metallicity in the bulge region than in the rest of our galaxies (and the opposite is true for the disc region).

We also find, in the bulge regions, a variety of [E/Fe] gradients, ranging from flat (NGC 1358), to positive (NGC 1433), to negative (NGC 1672 and NGC 1365), although the values at the very centre are always compatible with being zero. In particular, the decreasing [E/Fe] profile in NGC 1672 is due to the contrast between the bulge region and the inner disc region, where the stellar populations show a minimum in metallicity and [E/Fe]. The contrast between these two regions is also responsible for the positive age gradient and for the very steep metallicity gradient in the bulge region, where the star formation is proceeding from low-metallicity gas. The higher values of [E/Fe] and metallicity in the central region may be indicating that the star formation was more intense in the central region than in the circumnuclear ring (r) . The negative age gradient in NGC 1365 and NGC 1433 is also due to the contrast between the age in the bulge and that of the nuclear ring (r$\sim$19 arcsec for NGC 1433 and r$\sim$7 arcsec in NGC 1365).

7 CONCLUSIONS AND DISCUSSION

We are carrying out a project to understand the star formation history of disc galaxies and, in particular, the influence of the bar on producing large scale mixing in the stellar disc. In this paper we have tested the techniques we are planning to use to derive star formation histories and chemical evolution of disc galaxies using high quality, long-slit spectroscopy, for a sample of disc galaxies covering a range in mass and morphological type, with and without bars.

• To quantify the behaviour of the stellar population parameters we have derived the average values of age and metallicity weighting with the mass or the light of the stars. We discuss separately the results in the bulge and the disc region:

Bulge Region: In the bulge region, we have found that the age gradient depends on the presence of substructures such as circumnuclear discs or rings. This is in agreement with the results of Peletier et al. (2007), who found, using 2D line-strength maps, that the young stars are found either in rings or everywhere in the central regions. They also found that the presence of young stars is always associated with the presence of dust. This result is confirmed by studies of the morphology of star formation regions using Hα emission, that find Hα in circumnuclear regions such as inner rings and that relate the presence of these structures with the dynamics of the host galaxy and its stellar bar (Knapen 2005; Knapen et al. 2006). We believe, in agreement with Peletier et al. (2007), that the contradictory results obtained by different authors in relation to the age of the bulges are due to differences in the sample selection (barred or not barred) and inclination. For example, Jablonka et al. (2007) did not find any difference in the star formation history of barred and non-barred galaxies because their sample was edge-on and, therefore, they were not sensitive to the presence of nuclear discs or rings. Morelli et al. (2006) found very weak age gradients because their sample was selected to be non-barred. On the contrary, Moorthy & Holtman (2006) found different age gradients in barred and non-barred galaxies. In particular, they found that when positive gradients exist in their sample, they were invariably in barred galaxies.

The mass-weighted age in the bulge region is consistent with the disc and takes values of $\sim$10 Gyr, except in the very central region of NGC 1672 and NGC 1433. The bulge, as the disc, is dominated by old stellar populations. Similar results were obtained by MacArthur et al. (2009).

Inner Disc Region:

• The luminosity-weighted age gradient of the inner disc is always flat or slightly negative, compatible with a moderate inside-out formation. This result agrees with that obtained by MacArthur et al. (2009) for their sample of face-on galaxies or by Muñoz-Mateos et al. (2007) for a sample of nearby disc galaxies using a combination of UV and infrared colors. However, we only reach radii beyond corotation for half of the sample and, inside this radius, the stellar distribution and stellar population gradients might be significantly influenced by the bar potential. The moderate age gradient can be explained either by the disc not having grown very much in the last $\sim$8 Gyr, or if there has been radial mixing causing a migration of old stars to the external parts.

All the discs of our sample are dominated, in mass, by an old stellar population ($\sim$10 Gyr) and [M/H]~ -0.2 dex. This is true even at 3 scalelengths for some of our galaxies. This result agrees with studies of resolved stellar population in nearby disc galaxies like M81 (Williams et al. 2009) or NGC 300 (Gorgarten et al. 2010) where they found that, at 1.5-2 scalelengths, $\sim$70% of the stars formed 8 Gyr ago. However, in M33, a similar disc in morphology and mass seems to contain a much larger fraction of young stars at those distances (Williams et al. 2009). As Gogarten et al. (2010) suggest, these differences may be due to environment, as M33 is interacting with M31 (Braun & Thilker 2004; Bekki 2008). In contrast, NGC 300 and M81 are fairly isolated systems.

• Regarding the metallicity, we have found that the luminosity-weighted and mass-weighted metallicity gradients are very similar and always flat or slightly negative (NGC 1433) in the disc region. The mean metallicity in the disc is rather large, $-0.3 < [M/H] < -0.2$ dex. Together with the results of the item above, this indicates that most stars at $\sim$2 scalelengths formed at z>1 and experienced a rapid metal enrichment. These result coincide with those ob-

[4] Although nuclear rings have been detected in non-barred galaxies as well, see Knapen (2010).

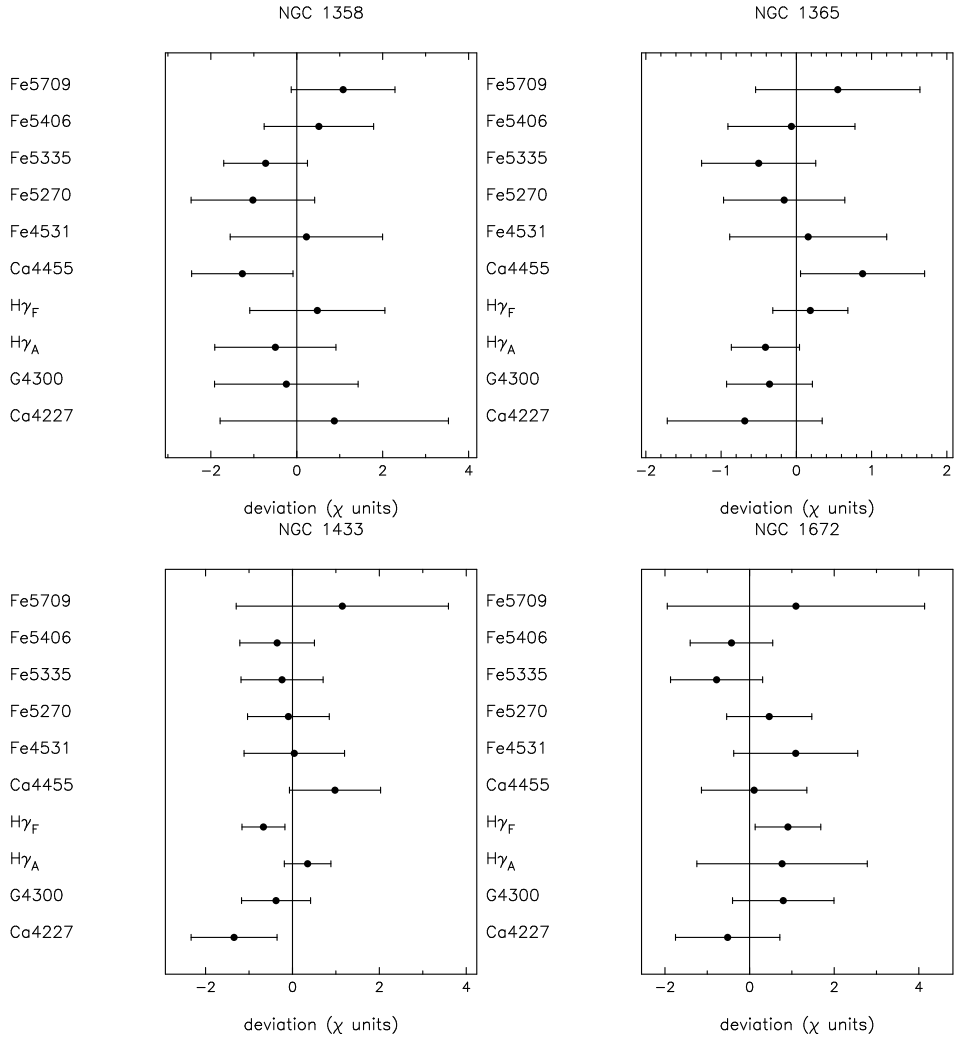

Figure 12. Average deviation in units of error (i.e., χ) of the measured indices from the indices corresponding to the best-fitting. Error bars represent the scatter in the deviation.

tained using resolved stellar populations in nearby discs – e.g., in M81 (Williams et al. 2009) and M31 (Brown et al. 2006).

• For two of the galaxies, NGC 1358 and NGC 1433 we have been able to compare the metallicity and age gradient along the disc with that along the bar, observed previously by Pérez et al. (2009). We have found that, in comparison with the stellar population in the disc, bars show older ages, higher metallicities, high [E/Fe] abundances and flatter gradients in both parameters. This finding argues against a recent formation of the bar from disc stars. As the stars in the bar are old, this results is a clear indication that, at least in some galaxies – the two galaxies analysed here are both early-types– this structure is old, giving a definitive answer to a long-standing controversy regarding the survivability of bars. This was already suggested in Pérez et al. (2008, 2009) and Gadotti & Souza (2006).

• We have found that the degeneracy between metallicity and σ in methods where the kinematics is determined at the same time as the stellar population parameters can seriously bias the final results. In particular, the mass-weighted metallicity tend to be higher than what it should be. This is true, not only when using our code, but also when other methods, as `starlight` is used. Therefore, we recommend calculating the kinematics separately by other methods and then fitting for the stellar population parameters. We also find that the age-metallicity degeneracy is highly reduced when `steckmap` is used to derived these parameters as opposed to the most classical index-index or multi-indices approaches.

• Despite the strong degeneracy between the age and metallicity when these parameters are derived using line-strength indices, the gradients are not very different from the luminosity-weighted values obtained with `steckmap`.

Previous studies using broadband colors (e.g. Bell & de Jong 2000) concluded that colour gradients were predominantly due to a gradient in metallicity. MacArthur et al. (2004) however, found both a gradient in age and metallicity and found that galaxies with stronger metallicity gradients are those showing flatter age gradients and vice-versa, showing the difficulty in breaking the age-metallicity-dust degeneracy using only broad-band colours. These different results do not invalidate a specific technique, but show the importance of interpreting correctly the results depending on the method used to obtain stellar population parameters.

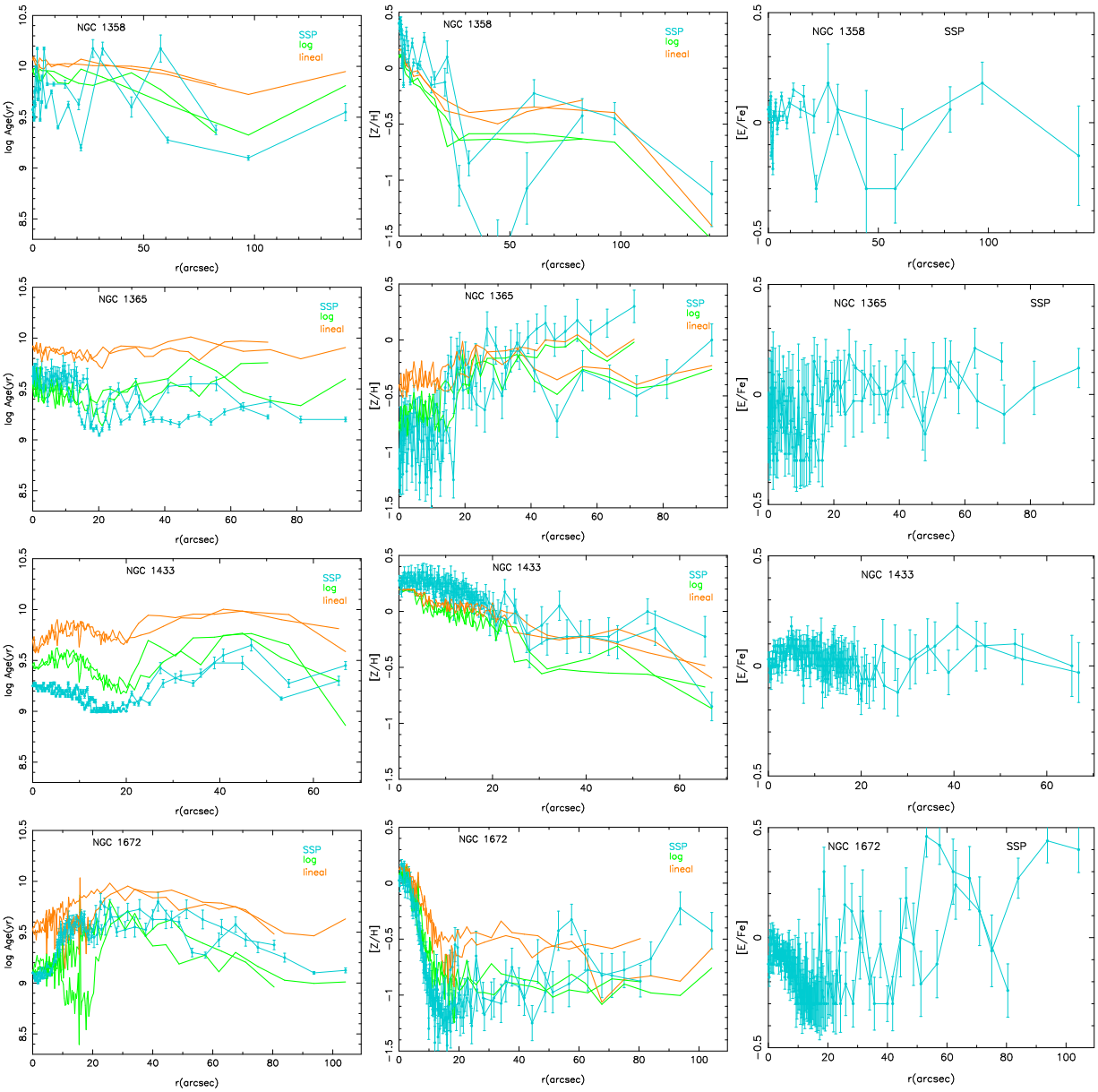

Figure 13. Single stellar population equivalent age, metallicity, and [E/Fe], as a function of radius for the galaxies of the sample.

In a following paper we will apply the techniques presented in this paper to study the differences in the star formation history of barred and non-barred galaxies.

ACKNOWLEDGMENTS

PSB is supported by the Ministerio de Ciencia e Innovación (MICINN) of Spain through the Ramon y Cajal programme. PSB also acknowledges a ERC within the 6th European Community Framework Programme. PO is supported by a grant form the French Centre National de Recherche Scientifique. BKG acknowledges the support of UK Science & Technology FacilitiesCouncil (STFC Grant ST/F002432/1) and the Commonwealth Cosmology Initiative. IP thanks the support of a postdoctoral fellowship from the Netherlands Organisation for Scientific Research (NWO, Veni-Grant 639.041.511) and she is currently supported by the Spanish Plan Nacional del Espacio del Ministerio de Educación y Ciencia(via grant C-CONSOLIDER AYA 2007-67625-C02-02). She also thanks the Junta de Andalucía for support through the FQM-108 project.

REFERENCES

Athanassoula E., 2003, MNRAS, 341, 1179
Barbanis B., Woltjer L., 1967, ApJ, 150, 461
Barker M. K., Sarajedini A., 2008, MNRAS, 390, 863
Beauchamp D., Hardy E., 1997, AJ, 113, 1666
Bell E. F., de Jong R. S., 2000, MNRAS, 312, 497
Binney J., Lacey C., 1988, MNRAS, 230, 597
Bruzual G., Charlot S., 2003, MNRAS, 344, 1000
Cappellari M., Emsellem E., 2004, PASP, 116, 138

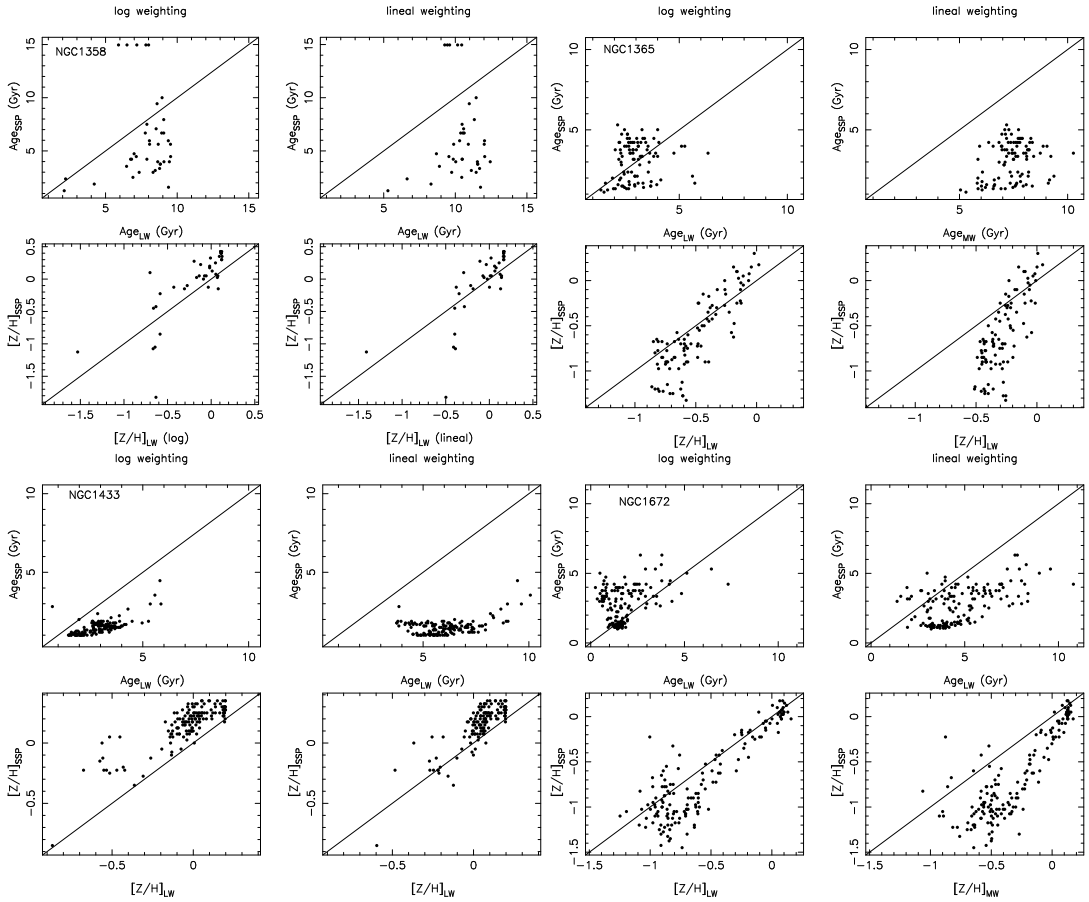

Figure 14. Comparison of the SSP-equivalent parameters and the luminosity- and mass-weighted values for the 4 galaxies of this study.

Cardiel N., 1999, PhD thesis, , Universidad Complutense de Madrid, Spain, (1999)

Carraro G., Geisler D., Villanova S., Frinchaboy P. M., Majewski S. R., 2007, A&A, 476, 217

Carraro G., Ng Y. K., Portinari L., 1998, MNRAS, 296, 1045

Cenarro A. J., Peletier R. F., Sánchez-Blázquez P., Selam S. O., Toloba E., Cardiel N., Falcón-Barroso J., Gorgas J., Jiménez-Vicente J., Vazdekis A., 2007, MNRAS, 374, 664

Chilingarian I., Prugniel P., Sil'Chenko O., Koleva M., 2007, in Vazdekis A., Peletier R. F., eds, IAU Symposium Vol. 241 of IAU Symposium, NBursts: Simultaneous Extraction of Internal Kinematics and Parametrized SFH from Integrated Light Spectra. pp 175–176

Cioni M., Irwin M., Ferguson A. M. N., McConnachie A., Conn B. C., Huxor A., Ibata R., Lewis G., Tanvir N., 2009, A&A, 500, 1025

Coelho P., Bruzual G., Charlot S., Weiss A., Barbuy B., Ferguson J. W., 2007, MNRAS, 382, 498

Coelho P., Mendes de Oliveira C., Cid Fernandes R., 2009, MNRAS, 396, 624

Crocker D. A., Baugus P. D., Buta R., 1996, ApJS, 105, 353

de Jong R. S., 1996, A&A, 313, 377

Debattista V. P., Mayer L., Carollo C. M., Moore B., Wadsley J., Quinn T., 2006, ApJ, 645, 209

D'Onofrio M., Zaggia S. R., Longo G., Caon N., Capaccioli M., 1995, A&A, 296, 319

Dumas G., Emsellem E., Ferruit P., 2007, in M. Kissler-Patig, J. R. Walsh, & M. M. Roth ed., Science Perspectives for 3D Spectroscopy A 3D View of the Central Kiloparsec of the Seyfert Galaxy NGC 1358. pp 269–+

Edvardsson B., Andersen J., Gustafsson B., Lambert D. L., Nissen P. E., Tomkin J., 1993, A&A, 275, 101

Favata F., Micela G., Sciortino S., 1997, A&A, 323, 809

Feltzing S., Gonzalez G., 2001, A&A, 367, 253

Feltzing S., Holmberg J., Hurley J. R., 2001, A&A, 377, 911

Flynn C., Morell O., 1997, MNRAS, 286, 617

Freeman K., Bland-Hawthorn J., 2002, ARA&A, 40, 487

Friedli D., 1998, in D. Friedli, M. Edmunds, C. Robert, & L. Drissen ed., Abundance Profiles: Diagnostic Tools for Galaxy History Vol. 147 of Astronomical Society of the Pacific Conference Series, Mixing and Transfer of Elements by Triaxiality. pp 287–+

Friedli D., Benz W., Kennicutt R., 1994, ApJ, 430, L105

Friel E. D., Janes K. A., Tavarez M., Scott J., Katsanis R., Lotz J., Hong L., Miller N., 2002, AJ, 124, 2693

Fuchs B., 2001, MNRAS, 325, 1637

Ganda K., Falcón-Barroso J., Peletier R. F., Cappellari M., Emsellem E., McDermid R. M., de Zeeuw P. T., Carollo C. M., 2006, MNRAS, 367, 46

Ganda K., Peletier R. F., McDermid R. M., Falcón-Barroso J., de Zeeuw P. T., Bacon R., Cappellari M., Davies R. L., Emsellem E., Krajnović D., Kuntschner H., Sarzi M., van

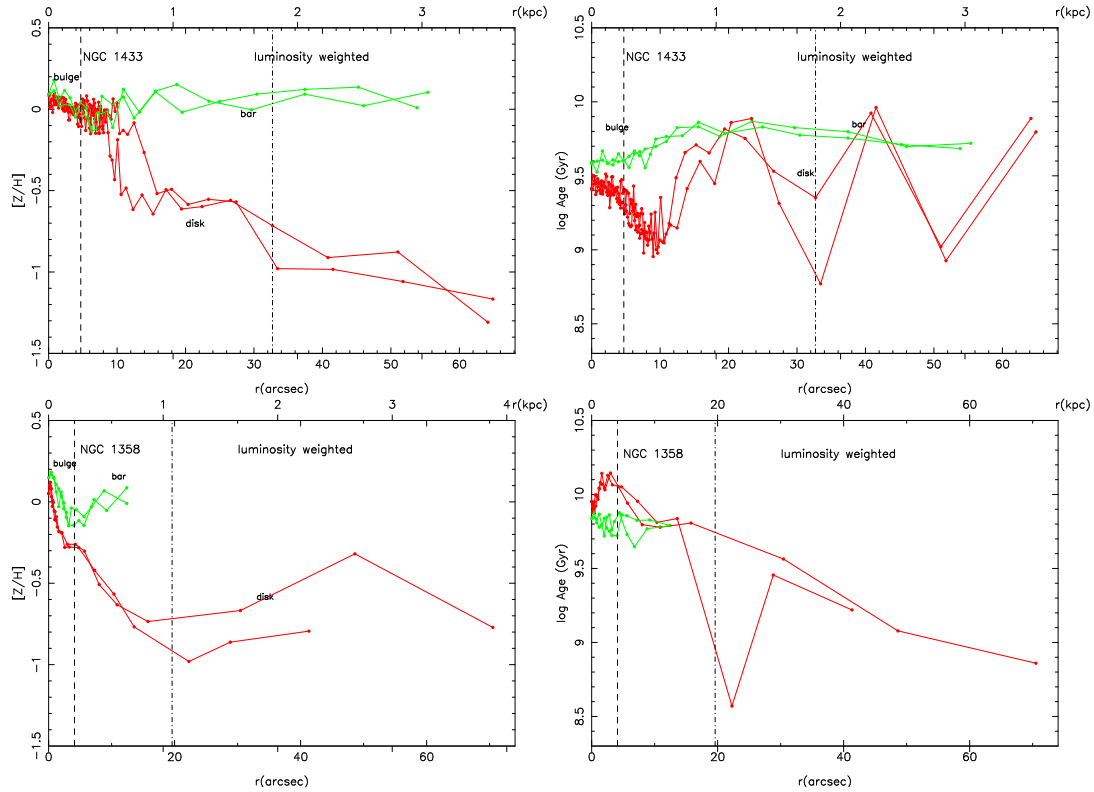

Figure 15. Luminosity-weighted ages and metallicities as a function of radius measured along the bar (green line) and along the major axis of the disc (red line).

de Ven G., 2007, MNRAS, 380, 506
Hameed S., Devereux N., 1999, AJ, 118, 730
Haywood M., 2001, MNRAS, 325, 1365
Hook I. M., Jørgensen I., Allington-Smith J. R., Davies R. L., Metcalfe N., Murowinski R. G., Crampton D., 2004, PASP, 116, 425
Houdashelt M. L., Trager S. C., Worthey G., 2005, Highlights of Astronomy, 13, 585
Knapen J. H., 2010, ArXiv e-prints
Koleva M., Prugniel P., Ocvirk P., Le Borgne D., Soubiran C., 2008, MNRAS, 385, 1998
Korn A. J., Maraston C., Thomas D., 2005, A&A, 438, 685
Le Borgne D., Rocca-Volmerange B., Prugniel P., Lançon A., Fioc M., Soubiran C., 2004, A&A, 425, 881
MacArthur L. A., Courteau S., Bell E., Holtzman J. A., 2004, ApJS, 152, 175
MacArthur L. A., González J. J., Courteau S., 2009, MNRAS, 395, 28
Maciel W. J., Costa R. D. D., Uchida M. M. M., 2003, A&A, 397, 667
Magrini L., Sestito P., Randich S., Galli D., 2009, A&A, 494, 95
Martin P., Roy J.-R., 1994, ApJ, 424, 599
Mollá M., Hardy E., Beauchamp D., 1999, ApJ, 513, 695
Monteverde M. I., Herrero A., Lennon D. J., Kudritzki R.-P., 1997, ApJ, 474, L107+
Ocvirk P., 2010, ApJ, 709, 88
Ocvirk P., Pichon C., Lançon A., Thiébaut E., 2006a, MNRAS, 365, 74
Ocvirk P., Pichon C., Lançon A., Thiébaut E., 2006b, MNRAS, 365, 46
Pagel B. E. J., Edmunds M. G., 1981, ARA&A, 19, 77
Pappalardo C., Lancon A., Vollmer B., Ocvirk P., Boissier S., Boselli A., 2010, ArXiv e-prints
Peletier R. F., Balcells M., 1996, AJ, 111, 2238
Peletier R. F., Falcón-Barroso J., Bacon R., Cappellari M., Davies R. L., de Zeeuw P. T., Emsellem E., Ganda K., Krajnović D., Kuntschner H., McDermid R. M., Sarzi M., van de Ven G., 2007, MNRAS, 379, 445
Pérez I., Sánchez-Blázquez P., Zurita A., 2007, A&A, 465, L9
Pérez I., Sánchez-Blázquez P., Zurita A., 2009, A&A, 495, 775
Pfenniger D., Friedli D., 1991, A&A, 252, 75
Proctor R. N., Forbes D. A., Beasley M. A., 2004, MNRAS, 355, 1327
Proctor R. N., Forbes D. A., Hau G. K. T., Beasley M. A., De Silva G. M., Contreras R., Terlevich A. I., 2004, MNRAS, 349, 1381
Rocha-Pinto H. J., Maciel W. J., 1996, MNRAS, 279, 447
Rocha-Pinto H. J., Maciel W. J., Scalo J., Flynn C., 2000, A&A, 358, 850
Roškar R., Debattista V. P., Quinn T. R., Stinson G. S., Wadsley J., 2008, ApJ, 684, L79
Ryder S. D., Fenner Y., Gibson B. K., 2005, MNRAS, 358, 1337
Sánchez-Blázquez P., Courty S., Gibson B. K., Brook C. B., 2009, MNRAS, 398, 591
Sánchez-Blázquez P., Gorgas J., Cardiel N., González J. J., 2006a, A&A, 457, 787
Sánchez-Blázquez P., Gorgas J., Cardiel N., González J. J., 2006b, A&A, 457, 809

Sánchez-Blázquez P., Peletier R. F., Jiménez-Vicente J., Cardiel N., Cenarro A. J., Falcón-Barroso J., Gorgas J., Selam S., Vazdekis A., 2006, MNRAS, 371, 703
Sarzi M., Falcón-Barroso J., Davies R. L., Bacon R., Bureau M., Cappellari M., de Zeeuw P. T., Emsellem E., Fathi K., Krajnović D., Kuntschner H., McDermid R. M., Peletier R. F., 2006, MNRAS, 366, 1151
Schiavon R. P., 2007, ApJS, 171, 146
Sellwood J. A., 1981, A&A, 99, 362
Sellwood J. A., Binney J. J., 2002, MNRAS, 336, 785
Sellwood J. A., Wilkinson A., 1993, Reports on Progress in Physics, 56, 173
Serra P., Trager S. C., 2007, MNRAS, 374, 769
Sérsic J. L., Pastoriza M., 1965, PASP, 77, 287
Sharina M., Davoust E., 2009, A&A, 497, 65
Spitzer Jr. L., Schwarzschild M., 1953, ApJ, 118, 106
Stanghellini L., Guerrero M. A., Cunha K., Manchado A., Villaver E., 2006, ApJ, 651, 898
Tantalo R., Chiosi C., Bressan A., 1998, A&A, 333, 419
Thomas D., Maraston C., Bender R., 2003, MNRAS, 339, 897
Toloba E., Boselli A., Cenarro A. J., Peletier R. F., Gorgas J., Gil de Paz A., Muñoz-Mateos J. C., 2011, A&A, 526, A114+
Trager S. C., Dalcanton J. J., Weiner B. J., 1999, in C. M. Carollo, H. C. Ferguson, & R. F. G. Wyse ed., The Formation of Galactic Bulges Integrated Stellar Populations of Bulges: First Results. pp 42–+
Trager S. C., Faber S. M., Worthey G., González J. J., 2000, AJ, 119, 1645
Treuthardt P., Salo H., Rautiainen P., Buta R., 2008, AJ, 136, 300
Tripicco M. J., Bell R. A., 1995, AJ, 110, 3035
Twarog B. A., 1980a, ApJS, 44, 1
Twarog B. A., 1980b, ApJ, 242, 242
Vazdekis A., 1999, ApJ, 513, 224
Veron-Cetty M., Veron P., 1986, A&AS, 66, 335
Vila-Costas M. B., Edmunds M. G., 1992, MNRAS, 259, 121
Williams B. F., Dalcanton J. J., Dolphin A. E., Holtzman J., Sarajedini A., 2009, ApJ, 695, L15
Williams B. F., Dalcanton J. J., Seth A. C., Weisz D., Dolphin A., Skillman E., Harris J., Holtzman J., Girardi L., de Jong R. S., Olsen K., Cole A., Gallart C., Gogarten S. M., Hidalgo S. L., Mateo M., Rosema K., Stetson P. B., Quinn T., 2009, AJ, 137, 419
Wyse R. F. G., Gilmore G., 1995, AJ, 110, 2771
Yoachim P., Dalcanton J. J., 2008, ApJ, 683, 707
Yong D., Carney B. W., Teixera de Almeida M. L., Pohl B. L., 2006, AJ, 131, 2256

APPENDIX A: COMPARISON BETWEEN MILES AND BC03 STELLAR POPULATION MODELS

Figure A1 shows the difference between the luminosity- and mass-weighted ages and metallicities obtained with two different stellar population models, MILES (Vazdekis et al. 2010) and BC03 (Bruzual & Charlot 2003) as a function of radius. It can be seen that, despite for some radial bins the differences can be very large, in general they scatter around zero, and the gradients of the differences are compatible with being null. The largest differences are obtained for populations with ages younger than ∼3 Gyr (ie, the bulge region of NGC 1433 and the ring region in NGC 1672). This is, in principle, in agreement with the results of Koleva et al. (2008) although we can not explore the parameter space in a systematic way as it was done in that work. However, we do not find large differences for populations with subsolar metallicity, like for example in NGC 1365.

APPENDIX B: DEGENERACY BETWEEN σ AND METALLICITY

It has been known for a long time that the determined velocity dispersion of a galaxy spectrum depends on the spectral type and metallicity of the stellar template (ie., Laird & Levison 1985; Bender 1990; Koleva et al. 2007). A deeper absorption feature can be obtained by either increasing the metallicity or decreasing the broadening. This leads to degeneracies when trying to derive both parameters at the same time. Koleva et al. (2007) quantify this degeneracy as:

$$\delta(\sigma)/\sigma \sim 0.4 \times \delta([Fe/H]) \quad \text{(B1)}$$

with σ in km/s and [Fe/H] in dex - a 0.1 dex mismatch in metallicity results in a 4% error in the velocity dispersion.

In order to quantify the differences in the obtained parameters with and without fixing the kinematics, we have perform the calculations using both methods. Figure B1 shows the results of the mass- and luminosity-weighted mean metallicity profiles when the kinematics are not fixed, derived using `steckmap`. As can be seen, in all cases, the luminosity-weighted values are lower than the mass-weighted ones. This is very puzzling, in principle, because it is contrary to what is expected in a normal chemical evolution scenario.

To check if this behaviour is a systematic error or an artifact of the method we are using, we repeated the experiment using the code `STARLIGHT` (Cid-Fernandes et al. 2005) for one of our galaxies, NGC 1672. Although `STARLIGHT` uses the continuum shape of the spectrum to perform the analysis, we have removed it from both the templates and the galaxies, using spline fits to avoid the uncertainties due to dust extintion. Figure B2 shows the results. As can be seen, although the absolute values in some regions differ depending on the code that we use, the general shape of the gradients are very similar, independent of the method used to derive star formation histories. The way `STARLIGHT` and `STECKMAP` find the optimal solution is quite different and the similarity of the results lends support to our final conclusions. As can be seen in the figure, `STARLIGHT` also gives lower luminosity-weighted than mass-weighted metallicities, contrary to what would be expected in a normal chemical evolution scenario.

To understand this effect better, we compare, in Fig. B3, the mean stellar population parameters obtained fixing and without fixing the kinematics when running `Steckmap`. As can be seen, while the mean ages are very similar, the metallicities obtained in both cases show clear differences. The effect is larger for luminosity-weighted values than for the mass-weighted ones. The net result is that the luminosity-

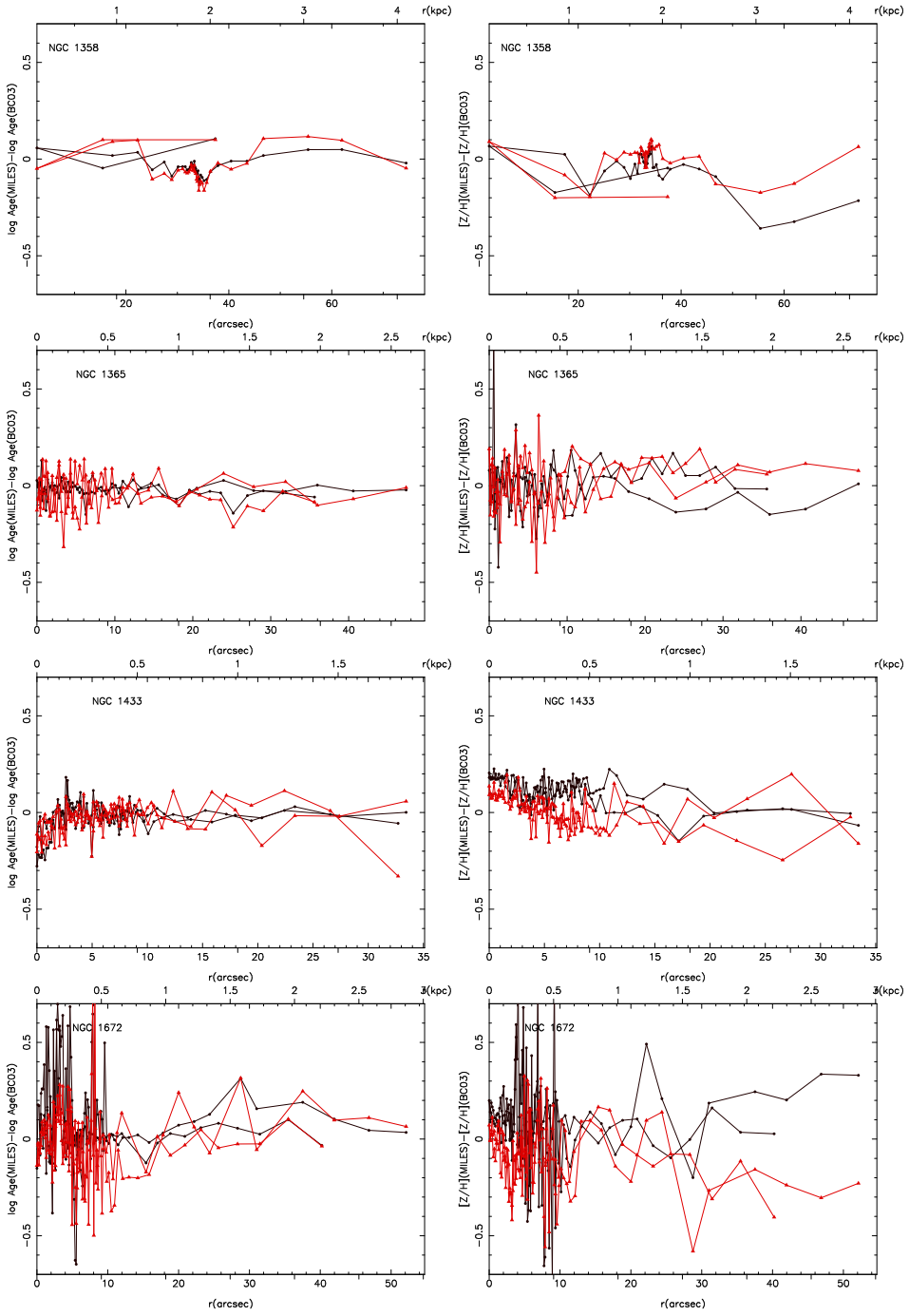

Figure A1. Differences in the luminosity-weighted (red) and mass weighted (black) mean age and metallicity obtained with the MILES and the BC03 stellar population models as a function of radius.

weighted metallicities appear to be lower than the mass-weighted ones.

The question then arises, how do we know which value is correct? We have mentioned previsouly that a scenario where the stellar metallicity decrease with time is, in principle, contrary to what would be expected for a standard chemical evolution scenario. However, this by itself is not an argument to discard the result. For example, it has been claimed that in our own Milky Way there has been chemical dilution (see, e.g., Tsujimoto et al. 2010). These authors present a compilation of metallicities measured in Cepheids (aged of about 10 Myr) and open clusters older than 1 Gyr, finding that the metallicity of the latter is higher than that of the Cepheids in the inner disc (up to more than four scale-lenghts), although the trend seems to reverse at larger distances. They are able to reproduce this evolution in metallicity with a model where the inner disc stars form from a metal enriched wind originating from the bulge. This wind is metal rich due to early efficient star formation. Later, accretion of low-metallicity gas from the halo dilutes the metals of the disk, producing a decreasing metallicity with time.

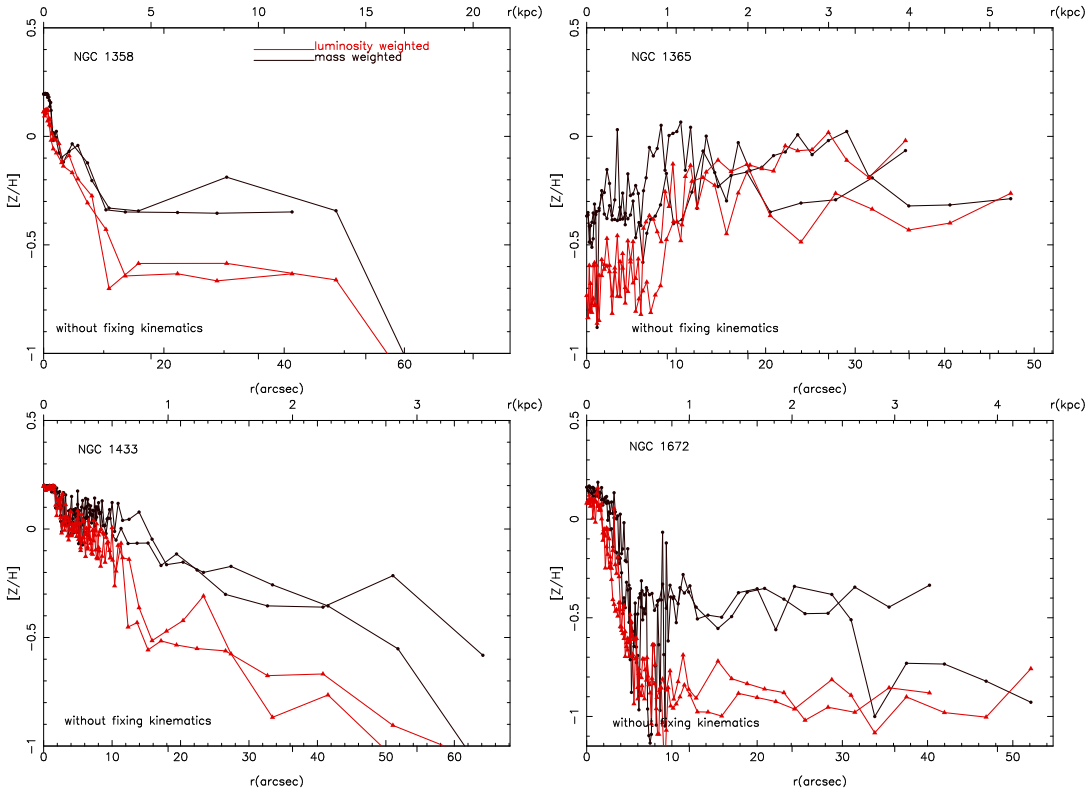

Figure B1. Mass- and luminosity-weighted metallicity gradients derived from the recovered star formation history, when the kinematics are not fixed

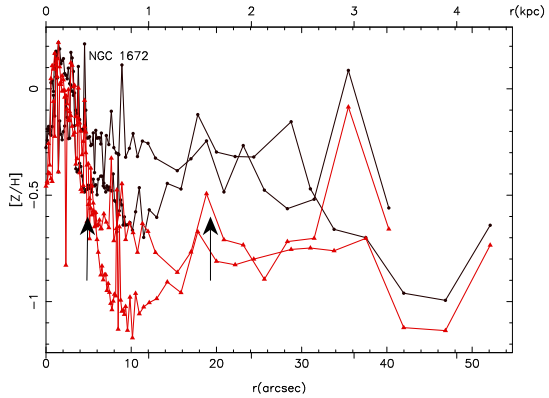

Figure B2. Mass- (black line) and luminosity-weighted (red line) age and [Z/H] gradients derived from the recovered star formation history using `STARLIGHT`.

To explore the systematics associated when the kinematics are fixed, as opposed to when it is not, under different evolutionary scenarios, we have performed a series of simulations. For these simulations we used an exponentially declining star formation history $\exp(-t/\tau)$ with different values of τ. The SSP models were truncated at ages$= [0.3-17]$ Gyr and the metallicities were chosen so as to remain in the $[\mathrm{Z/H}] > -1$ regime, to ensure that we work in a parameter space where the models are most reliable, and also to ensure that we bracket the parameter space covered by the galaxies we analyse. We have tested three different chemical enrichment scenarios. In the following equations t can be regarded as the age of the corresponding stellar component or the lookback time in Gyr.

(i) *Standard chemical enrichment*:

$$[\mathrm{Z/H}] = +0.2 - 0.51 \times (\log(t) + 0.5)\,. \qquad \text{(B2)}$$

In this model the youngest stars have $[\mathrm{Z/H}] = +0.2$, and the oldest stars have $[\mathrm{Z/H}] = -0.7$.

(ii) *no chemical evolution*: $[\mathrm{Z/H}] = 0$ (i.e. solar metallicity) for all the generations of stars.

(iii) *Reverse chemical evolution* or chemical dilution:

$$[\mathrm{Z/H}] = -0.7 + 0.51 \times (\log(t) + 0.5)\,. \qquad \text{(B3)}$$

In this model the youngest stars have $[\mathrm{Z/H}] = -0.7$ while the oldest stars have $[\mathrm{Z/H}] = +0.2$.

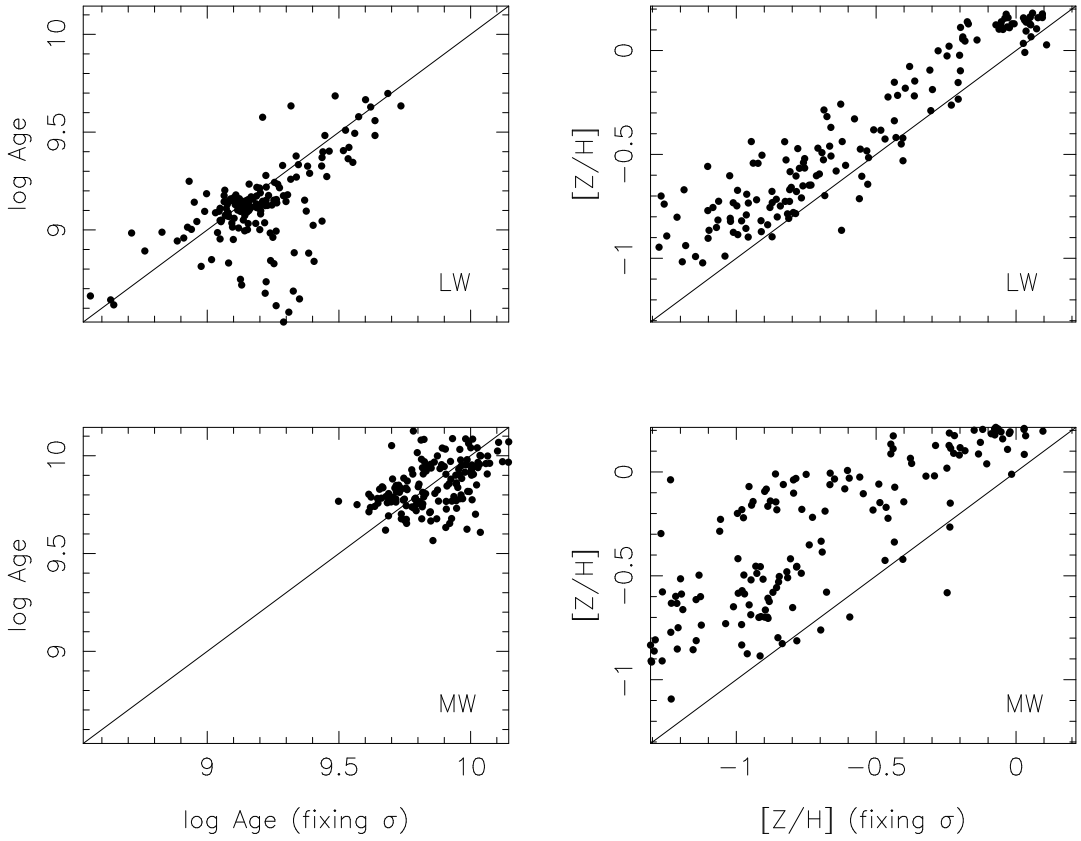

Figure B3. Comparison of the stellar parameters obtained when the σ is fixed and calculated using `Steckmap`.

We have used, for this experiment, the models by V10, broadened to 200 km/s. In order to mimic the data, we have added noise to the spectra to reach a signal-to-noise per Angstrom of 50. Figure B4 shows the difference between the luminosity- and mass-weighted metallicities as a function of τ for the three chemical evolution scenarios in both cases, when the kinematics is fixed and when it is not. The thick grey lines show the model for the 3 different scenarios, and the symbols are the values as computed from the `STECKMAP` inversions of the mock spectra. The error bars in the figure are computed as the RMS dispersion of the values obtained in 50 MonteCarlo simulations in which each pixel of the synthetic spectrum was modified randomly following a Gaussian distribution with a width given by the noise spectrum.

As can be seen, when the kinematics are fixed the difference between the luminosity- and the mass-weighted metallicity are much better reproduced than when the velocity dispersion is calculated at the same time as the stellar population parameters. As the effect is stronger for young ages and at larger metallicities, the "standard chemical evolution" scenario where the younger populations are more metal rich is the one that is more affected. This is the reason why when the σ is not fixed, we tend to get lower luminosity-weighted than mass-weighted metallicities.

B1 Testing the velocity dispersion

There was a concern, raised by the referee, that the kinematics we are measuring could be biased as we have used the same SSP-models than those used in `steckmap`, suggesting than the template mixing process behind the `pPXF` kinematics fit may well suffer from the same degeneracy that we are trying to avoid. To deal with this possibility we have perform two different tests:

(i) We have re-calculated the kinematics using a subset of the MILES stellar library, instead of the stellar population models. We have selected 250 stars coveraing a wide range in the atmospheric parameters and run `pPXF` using these as a templates. The results can be seen in Fig. B5. The offset between the velocity dispersions measured with the models and the stars is $-0.36 \mathrm{kms}^{-1}$ with an RMS dispersion of 12.6 kms^{-1}. That is, there is not a significant difference between the two values.

(ii) We have studied the impact that the errors in the measured σ have in the `steckmap` results. To do this we have run `steckmap` fixing the kinematics to the values of $\sigma + e\sigma$ and $\sigma - e\sigma$ for one of the galaxies, NGC 1672, where $e\sigma$ represent 1.5 of the formal errors. The results are displayed in Fig. B6. In the figure we show the mean stellar population parameters obtained in each case. It can be seen that the errors in the derived σ does not affect significatively the results of this work.

B2 Dependence of the Results on the Initial Guess and Best Initial Parameters

All iterative optimisation methods require a starting point, which is usually referred to as the 'initial guess'. Ideally, the method is insensitive to the choice of this guess, which is

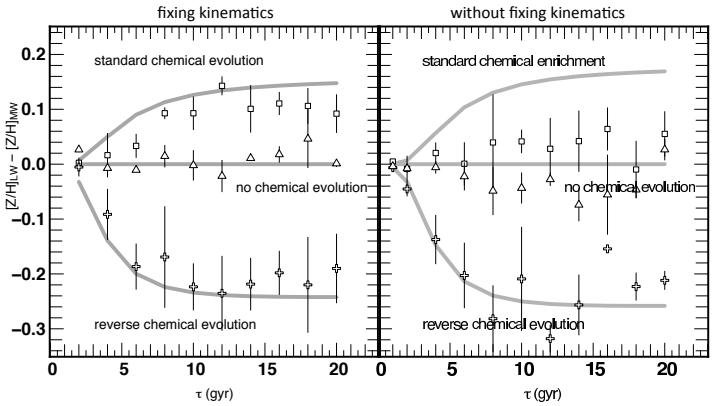

Figure B4. Differences between the mass and luminosity-weighted metallicities for exponentially declining star formation histories with various timescales τ (x-axis) generated as explained in Sec. 5.3 for three different chemical evolution scenarios. The thick grey lines are the values obtained from the models, and the symbols show the values recovered by `STECKMAP` fixing the kinematics (left panel) and without fixing it (right panels). The error bars are obtained via Monte Carlo simulations.

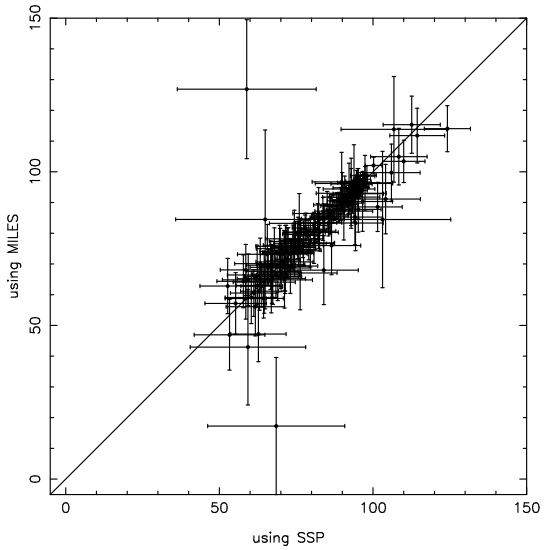

Figure B5. Comparison of the velocity dispersions using the SSP-models by V10 as templates and using a subset of 250 stars from the MILES library.

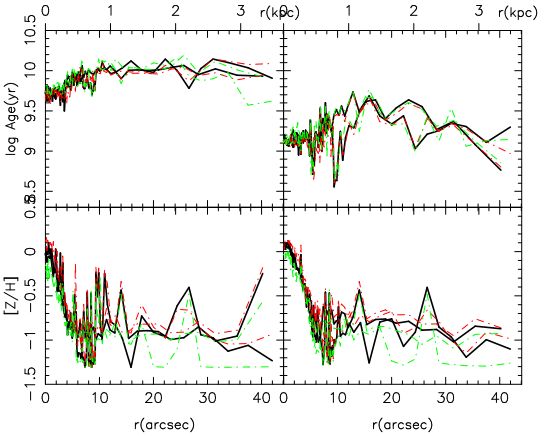

Figure B6. Mass (left panels)- and luminosity- (right panels) weighted ages and metallicities for the galaxy NGC1672 fixing the kinematics to the observed values (solid black line) and fixing the kinematics to σ+error in σ (red dashed line and σ-error in σ (green dashed line).

rather arbitrary. We have used for our real data an initial guess consisting of flat distributions for all fields. The reason for this choice is that it always converges to a good solution

(in the χ^2 and regularization sense), which is not true with all the first guesses. However, a bad choice for an initial guess can lead to bad fits or to secondary minima. To be sure that we reach a global minimum and not a secondary minimum, we have run `Steckmap` over several spectra using a family

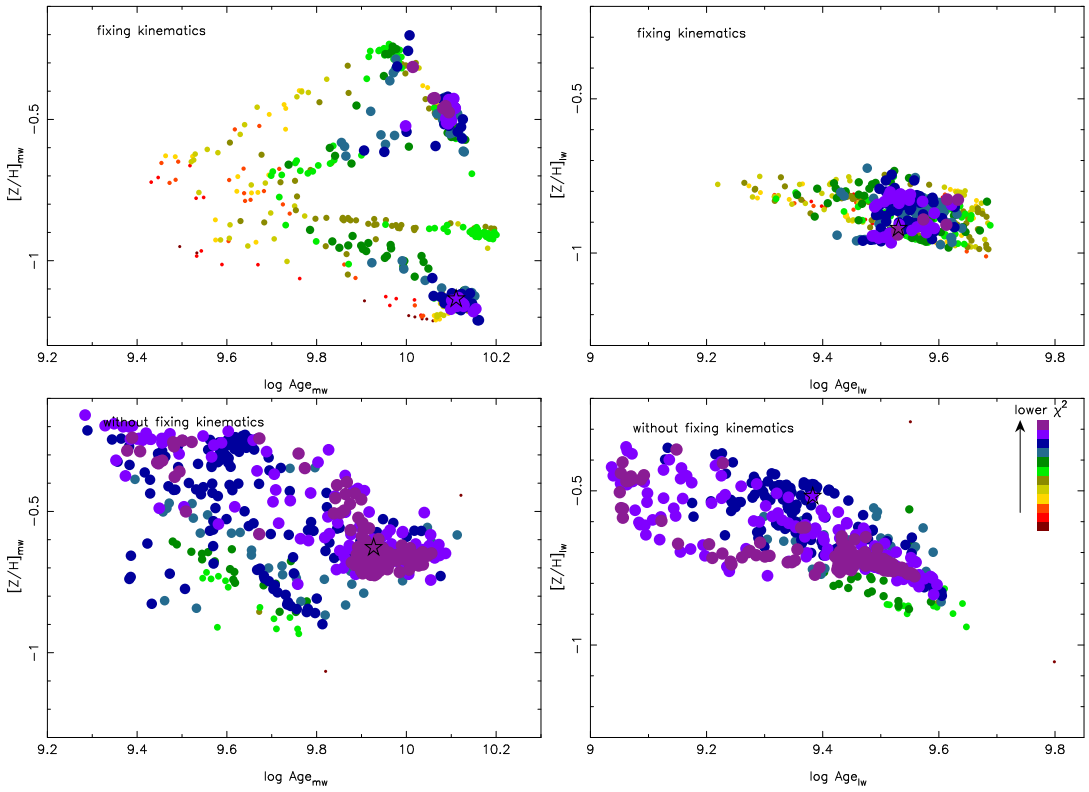

Figure B7. Luminosity- and mass-weighted metallicity vs. age for different Monte Carlo realisations, each with a different initial guess for `steckmap`. The initial guesses that we have used here consist of random bursts of star formation with random age and metallicity. The empty star shows the location of the solution found with the **flat initial guess**. This experiment was performed for galaxy NGC 1672 at position R=10.2 arcsec

of initial guesses. Here we show the experiments with first guesses consisting of random bursts happening at random times and with random widths. The age-metallicity relation of the model is flat with a random metallicity within the range of the models and the broadening function is a Gaussian centred at zero. We have performed 500 simulations. Figure B7 shows the mean age-metallicity plane using the two weights, luminosity and mass, for the different realisations. We have colour-coded the symbols depending on the χ^2 of the fit. The χ^2 of the fit is also inverserly proportional to the size of the symbol. We show as well, for comparison, the position of the value calculated with an initial guess of a flat distribution. We have performed the experiment for the two cases of fixing and not fixing the kinematics. As can be seen, the results may depend considerably on the choice of fitting or not fitting the broadening function. In the first case, we usually obtain two local minima, although one of them is clearer than the other. Furthermore, this minimum always coincides with the values that we obtain using a flat distribution as the intial guess. In the case where we try to calculate the kinematics, there is a clear age-metallicity degeneracy, especially for the luminosity weighted values.

These tests validate the flat initial guess as a good choice, and therefore this approach was adopted for this work. It allows users to analyse real data without having to experiment with a family of initial guesses, to find the best minimum of χ^2.